Nanomechanics of Organic Layers and Biomenbranes

Gerard Oncins Marco

UNIVERSITAT DE BARCELONA

Universitat de Barcelona

Facultat de Química

Departament de Química Física

NANOMECHANICS OF ORGANIC LAYERS AND BIOMEMBRANES

Gerard Oncins Marco

TESI DOCTORAL

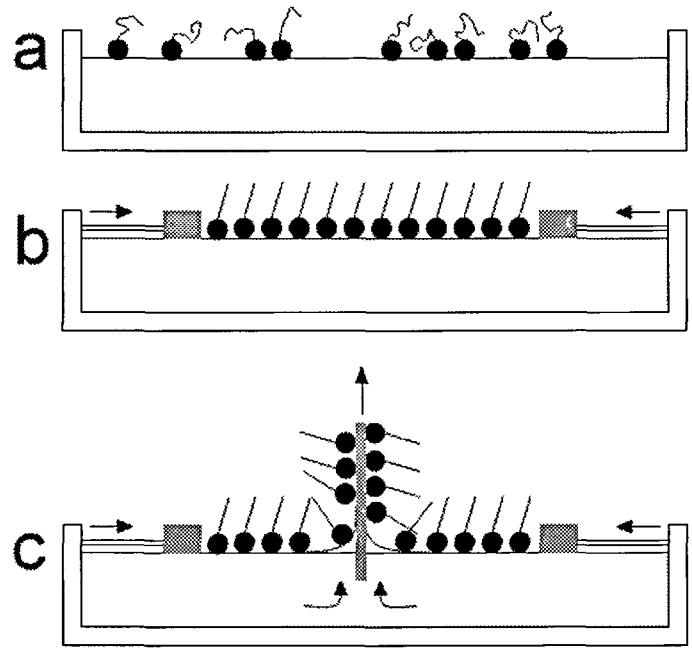

Fig. 25. Formation of a fatty acid LB film. a) The molecules accumulate in the liquid surface with the carboxylic acid groups towards the liquid and the hydrophobic chains towards the air. b) Two barriers compress the molecules while the surface pressure (π) is controlled. Before transferring the molecules to the solid surface, the film is called Langmuir monolayer. c) At the desired π value, the mica emerges from the liquid and the fatty acid molecules get stuck to its surface because of electrostatic interactions. The barriers compress the remaining monolayer so as to maintain a constant π value as molecules are removed from the liquid surface. Note that along with the molecules, water and cations are also transferred to the mica surface, conditioning the mechanical properties of the LB film.

4.5.4.1 Structure

As one of our ultimate motivation is to understand the relationship between nanotribology and structure, I would like to begin this section with the paper released by Kajiyama et al.[233], where the atomic lattice of LA and AA LB films and their hexagonal arrangement was resolved by AFM. They confirmed that the molecular area of the Langmuir monolayer, that is, the monolayer on the liquid surface before transferring it to the solid substrate, corresponds with the molecular area of the supported LB film. This is a very important fact, because it is mandatory to control the molecular area of the extracted monolayers and ensure that the structure and molecular area of the fatty acid on the mica surface is the same as in

the LB trough so as to obtain meaningful results. Concerning the position of individual molecules, Mori et al.[235] studied AA monolayers by AFM to conclude that molecules arrange perpendicularly to the substrate when the monolayer is extracted at 25 mN/m, which is in the boundary between liquid condensed (LC) and the solid (S) phase, as it can be seen in the isotherm depicted in Fig. 26. Interestingly, they also noted that it was not possible to obtain molecular perpendicularity when compressing an octadecyldimethylamine oxide monolayer, attributing this fact to steric effects due to the bulky amine polar head and its high degree of hydration. Besides, the issue of the hydrogen bonds established between the carboxylic polar heads was introduced[236], as well as the pH conditions that favor this interaction.

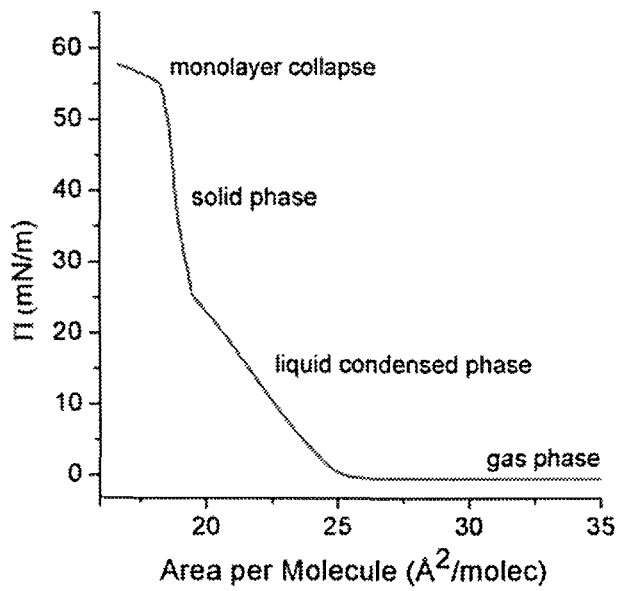

Fig. 26. π vs. area per molecule isotherm while compressing an AA monolayer in the LB trough. In the gas phase, the molecules can be compressed without increasing π. As intermolecular interactions grow stronger, the gas phase monolayer moves to the LC phase and, finally, to S phase. When a certain threshold π value is reached, the monolayer collapses and multilayers are formed, so the area per molecule is no longer meaningful.

Posterior works concerning the angle between AA molecules and the water subphase in Langmuir films reported that, while at an extraction pressure (π) of 50 mN/m the molecules are perpendicular to the liquid surface, the angle decreases for lower π values and the molecules pack in an orthorhombic system[231]. It was also

concluded that the transferring process to a solid substrate does not affect the lattice and the intermolecular distance, although previous X-ray studies of the same kind of layers maintained that the intermolecular distances on the supported monolayer were always the same, irrespectively of the Langmuir monolayer phase[237]. In conclusion, the results seemed to be contradictory and there was not a consensus in the scientific community about the validity of transferring a Langmuir monolayer to a solid substrate without changing the molecular packing. There was still quite a lot of work to do.

4.5.4.2 Effect of the pH and ions presence in the subphase

As fatty acids strongly depend on the interactions between their polar heads to structure themselves, pH and the presence of ions are extremely important factors, as they can modify the equilibrium of protonation-deprotonation of the carboxylic acids and the electrostatic interactions between them. A nice experimental prove of these concepts is the skeletonization of fatty acid LB films[238]; at certain conditions, AA monolayers form stripes perpendicular to the extraction direction that can be several micrometers width. Moreover, the grooves are only formed at a pH ~5.7 (the pKa of the AA is 5.4[239]) and with a certain concentration of Cd^{2+} in the subphase. The effect of cations had been previously shown by Outka et al. in a pioneering paper[214] where, depending on the cations present in the subphase (Cd^{2+} or Ca^{2+}), arachidate monolayers tilted around 33° or stayed perpendicular to the surface. Interestingly, this work was the base for the hydrocarbon chains interlocking proposed by Ulman et al.[213] regarding alkanethiols, applied to alkylsilanes by Kopta et al.[240] and refined with 2 dimensional interlockings by Barrena et al.[218] A systematic study concerning cadmium arachidate (CdAr) monolayers showed that their quality strongly depends on the pH, pointing out several key factors[241]; first of all, it must be considered the pKa of the substrate, in that case was mica, which strongly modifies the adhesion of cations on its surface[242]. Secondly, the pH can affect the complexation of the cations with the fatty acids carboxy- groups. In this sense, they observed that the

monolayer has more holes when the complexation is promoted and that the monolayer is more difficult to remove from the surface. This implies that the higher the complexation level, the smaller the molecular area, which translates into the creation of voids in the monolayer and the higher the mechanical resistance due to the interaction between the polar heads and the cations. Finally, the water layer that is present between the monolayer and the substrate has also to be considered, as it can modify the final monolayer structure once it has been transferred onto the substrate and influence the fatty acid molecular diffusion[243]. Sigiyama et al.[244] studied the LB isotherms of AA monolayers in the presence of different cations and concluded that the bigger the cation, the higher the intermolecular interaction, which eventually results in a higher collapse π value and a smaller intermolecular distance. Besides, they observed by means of AFM that the monolayers present domains that are thicker than the total length of the AA molecule and that they attributed to the formation of hydrated cations-AA complexes.

4.5.4.3 Nanotribology

In this section, I would like to separate two kinds of nanotribological works: those which use LFM as an imaging technique and those that use LFM to obtain mechanical properties of fatty acid films in a quantitative or semi-quantitative fashion.

4.5.4.3.1 LFM as an imaging technique

To begin with, LFM can be used as an imaging technique because the friction signal is very sensitive to different conformations or molecular structures[245], as it is shown in Fig. 27, which corresponds to a set of experiments that will be discussed in detail in the section 4.6.6. To begin with, I would like to mention one of the first works that exploited this technique; Meyer et al.[246] imaged cadmium arachidate multilayers and were able to discern between layers that shown their polar head (high F_f value) or their hydrophobic chain (low F_f value) to the AFM tip. As you may expect, this technique can be considered as an analytical tool and, in fact, the working principle has been strongly applied in the so-called

Chemical Force Microscopy[247,248]. It is also interesting to note that a mixture of lignoceric (LA) and palmitic acid (PA) revealed a strong LFM contrast[249]. In fact, one should expect a very similar response, as both fatty acid molecules are oriented with the hydrophobic chains towards the tip and only differ from the number of carbon atoms in the chain. Nevertheless, as each one of the two fatty acids was in a different phase, their structure was noticeably different, fact that stands for the observed friction contrast.

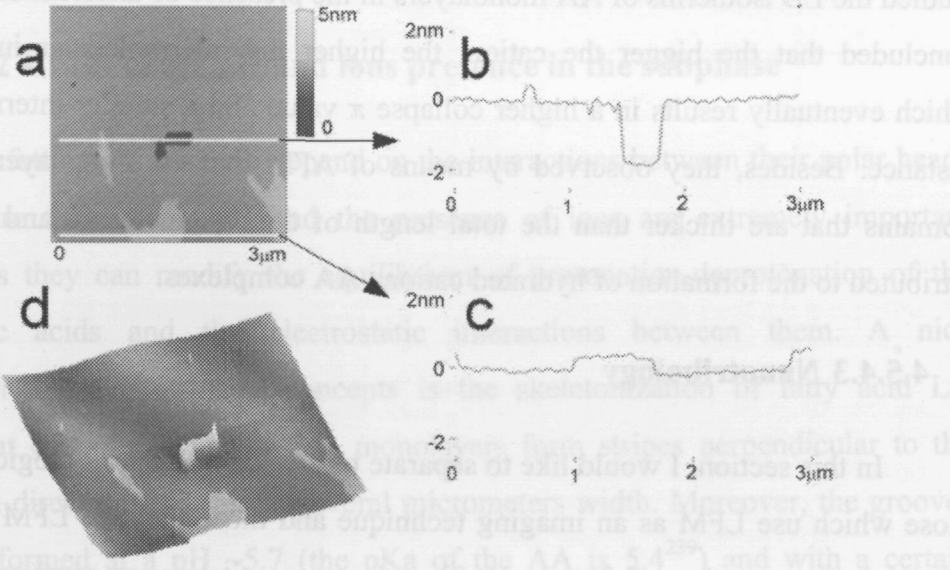

Fig. 27. Use of LFM as an imaging mode (original work in section 4.6.4). The sample is an AA LB monolayer extracted at 15 mN/m. A scratch has been performed in the center of the image to show the mica substrate. a) Topographic signal, where a continuous monolayer and domains can be appreciated (the discussion of this sample can be found in the section 4.6.4. b) Cross section of the image (white line) where the thickness of the monolayer can be measured. c) Cross section to reveal the height of the domains respect to the monolayer. d) 3D LFM image of the same area, where it can be seen that the higher F_f corresponds with the mica surface because of the hydrophilicity of both mica and AFM tip. The AA surface presents less F_f because it is –CH3 terminated but there is some friction contrast between the monolayer and the domains, demonstrating that LFM is not only sensitive to functional groups but also to structural differences (the domains and the monolayer only differ on the molecular area and tilting angle θ).

4.5.4.3.2 LFM quantitative experiments

Concerning quantitative friction experiments, it is remarkable the work released by Tsukruk et al.[250], who studied SA and cadmium stearate (CdSt)

monolayers and confirmed that hydrocarbon chain terminated monolayers render low F_f values while reverse monolayers, that is, when the polar heads point towards the air interface, present high friction when scanned with an AFM tip. This effect, observed in a more qualitatively way by Meyer et al.[246] for similar samples, may be understood in terms of the hydrophilic nature of Si_3N_4[70,251,252] and SiO_2[253] AFM tips. Consequently, the affinity between the tip and the polar heads is high, not only because electrostatic interactions but also because of the formation of water meniscus in ambient conditions[254-256]. The whole interaction results in a friction increment, as the tip is pulled against the surface and bends laterally while the two surfaces slide as depicted in Fig. 28. Concerning the durability of the samples, Tsukruk reported that a SA monolayer extracted at 20-35 mN/m shows some wear (detected by topographic AFM) when a F_v value of ~400 nN is applied. It has to be considered that the F_v value depends on the sliding velocity, but it is a good reference to understand the F_v range applied in this kind of experiments. Despite the quality of these measurements, perhaps the most interesting results come from the comparison of different samples extracted at different π values; strikingly, wear occurs at higher F_v values for CdSt extracted at 12 mN/m than for SA extracted at 20 mN/m. As we may expect, the higher the π value, the higher the F_v the monolayer can withstand without breaking (the molecules are packed more tightly so the monolayer is more difficult to disrupt). Nevertheless, the presence of carboxy- groups and complexing Cd^{2+} cations also reduces the molecular area due to the formation of strong electrostatic interactions and, as experimental results suggest, it can affect the nanomechanics of the fatty acids monolayers more than the mechanical compression process performed by the LB trough (Fig. 29). This effect can also be observed in LFM experiments, where μ value for CdSt is lower than for SA monolayers. Again, more compact monolayers show fewer defects and, consequently, fewer pathways for the sample to dissipate friction energy in the form of molecular deformation wit the consequent μ value diminution. Interestingly, the F_f signal inside the holes created after monolayer removing in wear experiments does not correspond with that of the clean substrate, so they proposed that the monolayer rupture does not remove whole patches of solid SA

molecules but it disorders and spreads the fatty acid molecules across the surface. When the wear experiments are performed on liquid SA monolayers (lower π values), the molecules do not pile up around the hole but they form multilayered structures. The deformation process itself is equally interesting; molecular dynamics simulations predicted that alkyl chains can be compressed up to 25% of their initial length before ongoing plastic deformation[191]. This fact was experimentally demonstrated measuring the monolayer thickness at variable F_v values, reporting tilting reversibility up to 60° angles. They also measured the monolayer force constant (k_m) and reported that when a F_v is applied on the monolayer, that is, while performing a nanoindentation experiment, k_m is ~100 nN/nm[257] while for a sliding contact, it ranges from 150 to 500 nN/nm. These results mean that the nanomechanical response of the monolayer is not the same when it is tested vertically or laterally and that LFM and Force Spectroscopy experiments probe different monolayer properties. In our works we have studied this point in more detail and we relate both the necessary F_v value to puncture the monolayer and the necessary F_v to disrupt the sample while performing LFM experiments with the molecular structure and interactions present in the layer (section 4.6.4).

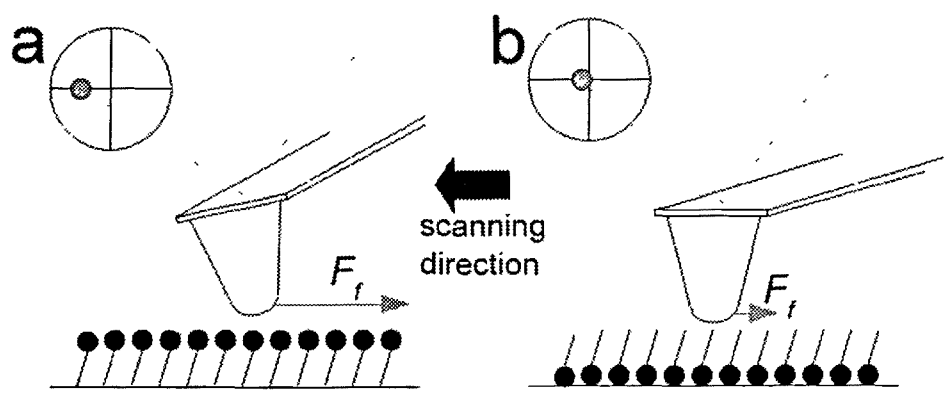

Fig. 28. Friction response of a fatty acid depending on the LB monolayer position. A) If the polar heads are shown to the air, the tip interacts with the sample by means of electrostatic, hydrophilic and water meniscus forces, resulting in a high F_f value. b) If the monolayer exposes its hydrocarbon tails to the air, (weak) van der Waals forces become dominant, giving rise to a low F_f value.

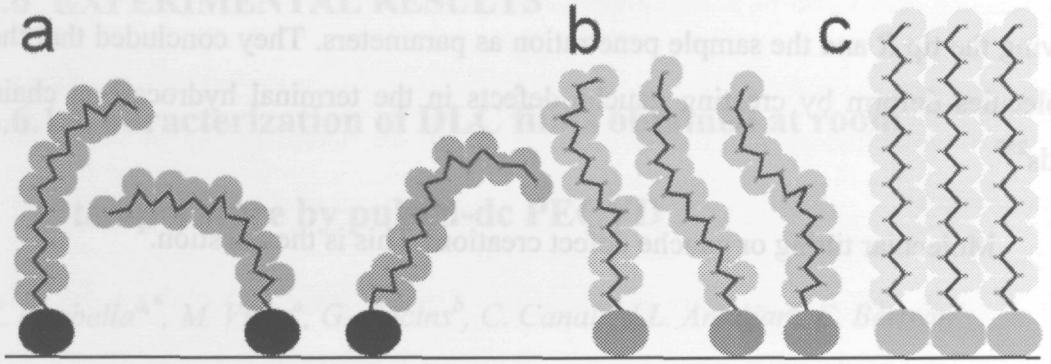

Fig. 29. Classic model that depicts the different molecular conformations for fatty acid monolayers as they are compressed in the LB trough. a) Gas phase, b) LC phase and c) S phase. Despite being a thoroughly accepted model, more recent results suggest that, although some gauche defects can be present in the molecular structure of fatty acids, the chains remain overall linear and change their tilting angle θ so as to maximize van der Waals interactions as presented in Fig. 24.

While Tsukruk et al. applied F_v values in the range of the hundreds of nN, Oishi et al.[258] performed LFM experiments on behenic acid (BA) monolayers applying a lower range of F_v values, just up to 10 nN, which explores in more detail the regime were the elastic deformation takes place. They discovered that, while BA monolayers in the solid phase firstly deform elastically and then plastically, the liquid monolayers deform plastically from the beginning. They explored this effect measuring the dependence of F_f value with the sliding speed to find non-dependence for the solid phase and a strong dependence in the liquid phase. They concluded that the nanotribological differences between the two phases were founded on structural dissimilarities, as molecules in liquid phase are more disordered and deform easily as F_v is applied. This leads to a plastic deformation, which increases A between sample and tip and promotes a further F_f increment. Besides, F_f is also enhanced by monolayer wear. On the other hand, the solid phase behaves differently as molecules pack tightly and can withstand certain pressure without disordering. While the F_v value does not reach the threshold, the monolayer deforms elastically and A remains more or less constant. A posterior work that studied the energy necessary to plastically deform the BA monolayers according to the energetic model proposed by Hartig et al.[221], calculated the energy applied by the tip on the sample at a certain F_v considering a Hertzian contact model and

having the tip R and the sample penetration as parameters. They concluded that the molecules deform by creating gauche defects in the terminal hydrocarbon chain ends[259].

Molecular tilting or gauche defect creation? This is the question.

4.6 EXPERIMENTAL RESULTS

4.6.1 Characterization of DLC films obtained at room temperature by pulsed-dc PECVD

C. Corbella[a,], M. Vives[a], G. Oncins[b], C. Canal[c], J.L. Andújar[a], E. Bertran[a]*

[a]FEMAN, Departament de Física Aplicada i ôptica, Universitat de Barcelona, Av. Diagonal, 647, E08028 Barcelona, Spain

[b]Serveis Científico-Tècnics, Universitat de Barcelona, PCB, C/Josep Samitier, I-5 E08028 Barcelona, Spain

[c]Departamento de Tecnología de tensiactivos, IIQAB-CSIC, C/Jordi Girona 18-26, E08034 Barcelona, Spain

Diamond and related Materials 13 (2004), 1494-1499.

4.6.1.1 Summary

In this work, DLC films were deposited on Si substrates by means of plasma-enhanced chemical vapor deposition (PECVD) at room temperature and studied by Langmuir probe, electron energy distribution function studies and current intensity vs. voltage curves. Our contribution to the work was to perform LFM measurements on DLC films obtained at different frequency, peak voltage values and humidity levels in order to assess the effect of these factors in the nanotribological properties of the films. As it was one of our first works in the field, we did not use the LFM setup shown in Fig. 14 but a somewhat simpler version; as the system that controls the linear increment of F_v value was not yet developed, the number of points in the F_v vs. F_f curves is limited, as the F_v value was incremented manually after recording the F_f signal. One of the accomplished

goals is that AFM probes were laterally calibrated, so F_f values shown in this work are quantitative.

The conclusions that can be extracted from the nanotribological studies can be resumed as:

- *At 0% RH, the μ value for the DLC films is independent from the peak voltage and frequency used to deposit them during the PECVD process. We concluded that the quality of the films is independent from these deposition parameters.*

- *At 70% RH, the μ value is considerably higher for all the tested deposition conditions. We concluded that, despite the hydrophobic nature of the DLC films, water can accumulate on its surface, probably on defects, forming water micro droplets that are dragged away by the AFM tip during scanning. As the tip is hydrophilic, the water interacts with its surface and the μ value increases.*

Available online at www.sciencedirect.com
SCIENCE DIRECT®
ELSEVIER
Diamond and Related Materials 13 (2004) 1494–1499
DIAMOND AND RELATED MATERIALS
www.elsevier.com/locate/diamond

Characterization of DLC films obtained at room temperature by pulsed-dc PECVD

C. Corbella[a,*], M. Vives[a], G. Oncins[b], C. Canal[c], J.L. Andújar[a], E. Bertran[a]

[a]FEMAN, Departament de Física Aplicada i Òptica, Universitat de Barcelona, Av. Diagonal, 647, E08028 Barcelona, Spain
[b]Serveis Científico-Tècnics, Universitat de Barcelona, PCB, C/Josep Samitier, 1-5 E08028 Barcelona, Spain
[c]Departamento de Tecnología de Tensioactivos, IIQAB-CSIC, C/Jordi Girona 18-26, E08034, Barcelona, Spain

Abstract

Diamond-like carbon films were prepared at room temperature from asymmetric bipolar pulsed-dc methane glow discharges, up to 1600 V of negative voltage pulse and 50–200 kHz of pulse frequency. Plasma parameters within a pulse cycle and at different peak voltage amplitudes were characterized by a Langmuir probe, which measured the *I–V* characteristics and the electron energy distribution function. Electron and ion density, electron temperature and averaged electron energy are found to increase along with negative peak voltage. Moreover, variations of electron temperature and density of charged species are registered between high- and low-pulse level. Meta-stable dissociation of methane was detected at electron energies of approximately 12 eV. Properties of the films are discussed as a function of the growth parameters obtained by plasma diagnostics, in order to establish their influence on film features. The deposition rate and residual stress of the film, which reached 50 nm/min and was minor than 1 GPa, respectively, were correlated to the enhancement of the degree of ionization at high power values. Surface topography shows an increase of roughness, up to 1 nm of RMS value, for films deposited at high peak voltages, whereas the friction coefficient, measured by atomic force microscopy in contact mode, is approximately constant. Surface energy was characterized by contact angle measures with water, which value is approximately 85°, and shows no dependence with deposition conditions. This deposition technique has an application in industry for deposition of large area coatings and it is especially indicated to process materials with plasma involving a great number of technological parameters.

Keywords: Diamond-like carbon; Surface characterization; Plasma CVD; Tribology

1. Introduction

Diamond-like carbon (DLC) films have been studied in depth over the last 20 years. Their production in either unhydrogenated amorphous carbon (a-C) or hydrogenated form (a-C:H) involves a great number of deposition techniques such as sputtering of a graphite target and plasma-enhanced chemical vapour deposition (PECVD), or plasma CVD, through a hydrocarbon discharge. Extensive reviews [1,2] have shown a strong relationship between growth conditions and physical properties of DLC films. In particular, the bias voltage applied to the substrate holder during deposition affects their microstructure and properties. The right choice of this parameter leads to films with diamond-like properties. The hardness of DLC films, their low friction coefficient and low wear rates so achieved suggest their performance in a great number of applications, which make DLC films attractive for materials engineering and justify the study of their production at industrial scale [3].

PECVD of insulating films requires the substrates to be powered with an alternating signal. In the case of DLC film deposition, the cathode signal is usually driven by an rf (13.56 MHz) source. Some drawbacks of this method can be overcome by high-power pulsed-dc suppliers. Compared to rf power processes, modern pulsed-dc technology provides higher deposition rates and does not require matching networks, resulting in a reduction of production cost. The analysis of DLC films obtained using this technology is reported elsewhere [4]. In this study, DLC films obtained by PECVD technique with a pulsed plasma have been characterized. The

*Corresponding author. Tel.: +34-93-403-7092; fax:: +34-93-402-1138.
E-mail address: corbella@fao.ub.es (C. Corbella).

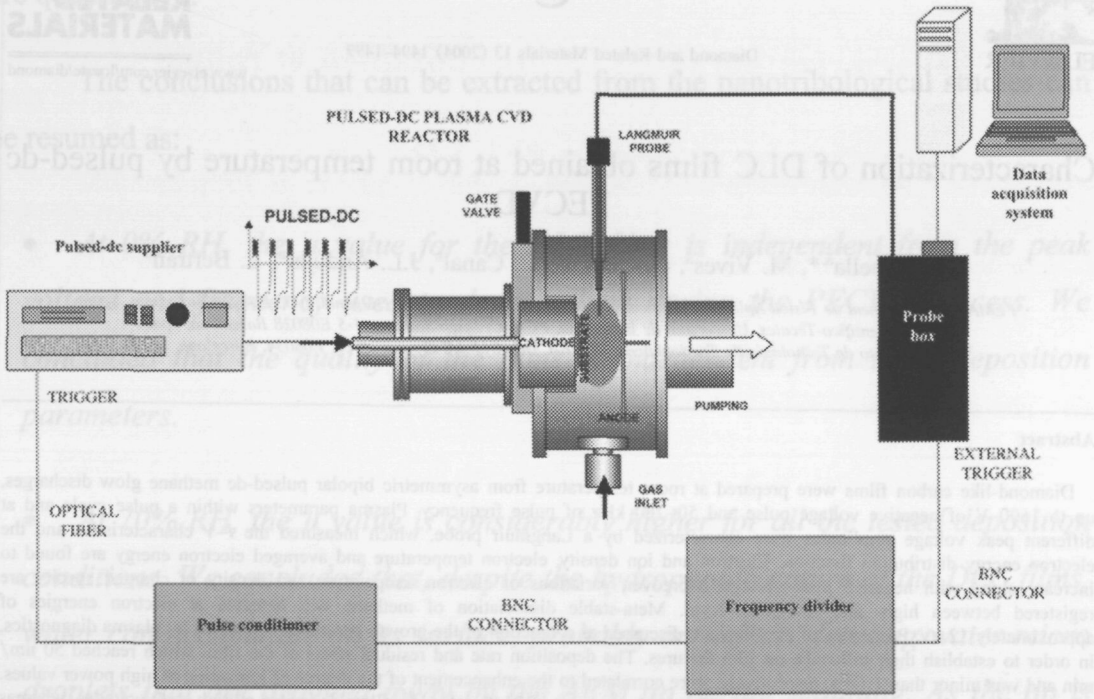

Fig. 1. Schematic of the experimental set-up for film deposition and plasma data acquisition.

deposition process was studied by analyzing the plasma features within a pulse cycle through a Langmuir probe. The growth rates and internal stresses were determined by profilometry. Some surface features, such as nano-friction coefficient, topography and surface energy (contact angle) are discussed in terms of plasma parameters during deposition.

2. Experimental details

The samples analyzed consisted of DLC films between 100 and 1000 nm thick, deposited on c-Si substrates placed on a water-cooled holder, by plasma CVD with a methane environment in a plasma reactor provided with a load-lock chamber, and a computer-controlled gas supply and pumping system. The power was supplied to the substrate holder by an asymmetrical bipolar pulsed-dc source (ENI RPG-50) that was operated in power regulation mode. The voltage waveform consisted of a fixed positive pulse amplitude of 40 V followed by a variable negative pulse whose peak amplitude varied from −600 to −1600 V. Pulse frequencies of 50, 100, 125, 150 and 200 kHz were used at a constant positive pulse of 2 μs, resulting in duty cycles of 90, 80, 75, 70 and 60%, respectively. The *I*–*V* characteristics of the plasma were determined by a SmartProbe (Langmuir probe) from Scientific Systems. A computer program provided plasma parameters (electron temperature, ion and electron densities and currents) and the electron energy distribution function (EEDF). The data acquisition system for plasma diagnostics was completed by a time delay circuit to scan current–voltage (*I*–*V*) characteristics within the pulse cycle (Fig. 1). All the depositions were performed at room temperature and at 10 Pa.

The film thickness was measured by surface profilometry. Stress was obtained by measuring the radius of curvature of the substrates before and after the deposition, and applying Stoney's equation. The surface topography measurements were performed by a Digital Instruments Nanoscope IV atomic force microscope (AFM) operating in tapping mode at 2 Hz in a scan area of 1×1 μm^2. Nano-tribology measurements were obtained by AFM scans of 200 nm length employing a Si_3N_4 cantilever (tip radius 100 nm) in contact mode, at 1 Hz. In order to reduce hysteresis on the piezoelectric actuators, scanning transversal to the long axis of the cantilever was preferred [5]. Average values of friction

Table 1
Plasma parameters measured in a 50 kHz pulsed-dc methane glow discharge at a pressure of 10 Pa. The plasma potential was 30 V

Peak voltage (V)	−1000		−1600	
Power (W)	32		100	
Pulse level	High	Low	High	Low
Electron density (10^9 cm^{-3})	3.45±0.06	12.0±0.4	5.24±0.01	29.3±0.5
Ion density (10^9 cm^{-3})	4.66±0.02	0.33±0.01	8.32±0.01	0.27±0.01
Electron temperature (eV)	1.84±0.02	0.85±0.02	3.05±0.03	2.73±0.03
Averaged electron energy from EEDF (eV)	2.8	1.3	4.6	4.1

coefficient were inferred from lateral to load force ratios obtained at different loads. Contact angle measurements were performed by the Wilhelmy plate method with a Sigma 20 tensiometer by dipping the samples in H_2O_{mq} (Milli-Q water) at a rate of 0.5 mm/min.

3. Results and discussion

I–V characteristics of the methane discharges were measured with a time resolution of 10 μs at a dc-pulse frequency of 50 kHz and a duty cycle of 90% (low power time of 2 μs). Thus, the average plasma diagnostics were obtained for different peak voltages distinguishing between high- and low-power levels within a pulse cycle (20 μs).

The plasma parameters measured at −1600 and −1000 V of bias peak voltages for pulse high and low levels are listed in Table 1. To obtain more accurate measurements, electron temperature was calculated from EEDF, and densities of ions and electrons were deduced from *I–V* curves [6]. In all the cases, a constant plasma potential of approximately 30 V was obtained for the whole cycle, suggesting a total recombination time of plasma species longer than 2 μs. The electron temperature at high pulse level (Table 1) reached 3 eV, whereas values less than 1 eV were registered at the low level. This result is consistent with Ref. [7], where an increase of the electron temperature at the start of each pulse was reported. The ion current, determined by the Langmuir probe, reached similar values of 0.3 mA at high level but disappeared practically (approx. 10^{-6} A) during the low pulse time. Ion density values at high power level doubled electron density, which indicates an electropositive plasma. This situation was reversed at a low pulse level, where electron density was 3×10^{10} cm^{-3}, two orders of magnitude above ion density, producing a strong deviation from the electrical neutrality of the discharge and an enhancement of the ionization. The observed increase in the electron density and the electron temperature with negative peak voltage has a considerable influence on the deposition rate of DLC films. Along with pulse power, it increases from <10 nm/min up to 50 nm/min at any pulse frequency [8], since the films grow faster in a more chemically active plasma. More recent studies have developed growth models considering the role of methyl and hydrogen bombardment [9]. These models require the previous knowledge of the distribution of the different ionized species, not determined here. However, an increase of deposition rate has been shown as linearly related to the energy per pulse [8], which is associated to the ionization degree (note the considerable increase of the ion density at high pulse level in Table 1).

Compressive stress of DLC layers decreased at all frequencies as the peak voltage increased. The lowest stressed films showed values below 1 GPa, whereas maximum stresses did not reach 2.2 GPa, which corresponds to DLC samples deposited supplying rf power. It is assumed that the reduction of stress could be due to the relaxation of carbon atoms and ions adsorbed onto the film surface during the low voltage positive pulses [8]. Therefore, as the increasing voltage bias leads to a more ionized plasma, more ions impinge on the film surface, making it less stressed.

Fig. 2a and b shows the EEDF at both power levels corresponding to values of −1600 and −1000 V of peak voltage at 50 kHz, respectively. These figures show that electrons follow a Druyvestein distribution, as expected for a plasma pressure of 10 Pa, where a collisional regime takes place:

$$n(E)=\frac{2I''_e}{eA}\sqrt{\frac{2mE}{e}} \quad (1)$$

In this expression [Eq. (1)], the electron energy $E=V-V_p$; V is the voltage applied to the probe and V_p is the plasma potential; I''_e is the second derivative of the electron current with respect to E; A is the probe surface area; m is the electron mass, and e is the electron charge. At 2 eV, the EEDF from Fig. 2b at high power level achieves a maximum value of 3×10^9 cm^{-3} eV$^{-3/2}$, and decreases exponentially down to 10^5-10^6 cm^{-3} eV$^{-3/2}$ for energies of 12 eV. At high power level, an increase of the population of energetic electrons with respect to the low level is also observed. This greater abundance of electrons is correlated to the enhancement

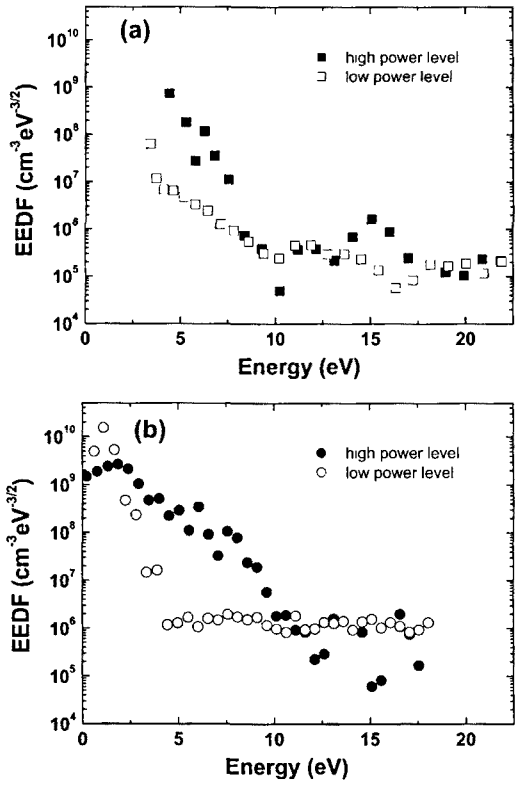

Fig. 2. EEDF corresponding to high- and low-power level of pulsed-dc plasma at peak voltages of: (a) −1600 V; (b) −1000 V.

of positive ionic current at high power level. Hence, more energetic electrons provide more efficient ionization, resulting in a positive ion-rich plasma. Moreover, as negative bias increases (Fig. 2a), the EEDF high values become restricted only for low energies. However, peaks of electron population appear at approximately 12 and 15 eV, indicating possible meta-stable dissociations of methane molecules in the glow discharge, since the electron impact dissociation threshold energy starts at approximately 10 eV [10]. Such dissociations lead to stronger dehydrogenation of methane molecules, and consequently to carbon-rich films. The increase of hydrogen ion bombardment so achieved may cause a H depletion in DLC film. Furthermore, this dehydrogenation may also proceed from surface–gas interactions, for example the removal of surface atomic hydrogen, through the dissociation of C–H bonds due to collisions with hydrogen or hydrocarbon radicals from the gas phase [9]. This fact agrees with the reduction in hydrogen bonding in the amorphous network as power increases, reported by Andújar et al. [8].

Fig. 3 shows the RMS surface roughness of DLC films measured by AFM as a function of the peak voltage from the pulsed signal. In general, at voltages from −600 to −1000 V the surfaces are smoothed. For higher negative voltages, roughness tends to increase. This roughening mechanism, more efficient at low frequencies, where the RMS value approaches 1 nm at −1400 V and 100 kHz, could be due to the increase of atomic hydrogen bombardment at high dc power. Actually, the average electron energy inferred from EEDF grows with a negative peak voltage (Table 1). It leads to a more ionized plasma, resulting in a higher atomic hydrogen etching on the growing film, which, in general, tends to cause surface roughening [11].

Nano-friction measurements were carried out by AFM in a dry atmosphere and in laboratory conditions. In order to avoid the influence of the tip radius on measures, we used a worn tip. In this way, the radius remained constant at different scans. Fig. 4 plots the lateral force vs. load force. Linear regression analysis on the slope of this plot yields the friction coefficient. The lateral force detected at zero load is attributed to a residual force of adhesion of the cantilever to the surface [12]. Fig. 5 plots the dependence of relative values of friction coefficient (not absolute values) with deposition conditions. No significant changes are observed when analyzing DLC samples prepared at different conditions in dry atmosphere. However, humidity enhances friction, as observed from the deviation of data points with respect to the dry conditions. The sample prepared at 200 kHz even shows a discrepancy of 100% between coefficients. When the scan takes place in moist conditions, a meniscus is formed between the hydrophilic Si_3N_4 tip and the microscopic water drops condensed on the hydrophobic surface of a-C:H. This may increase the lateral force during the scans, which explains the increase of the friction coefficient.

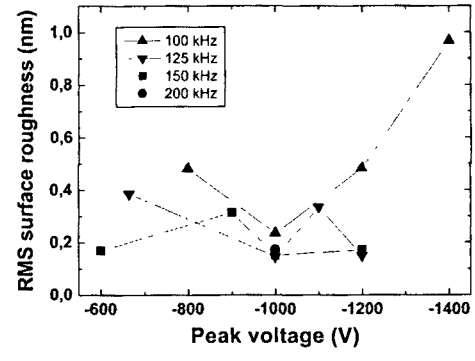

Fig. 3. RMS surface roughness of DLC films, deposited at different frequencies, as a function of peak voltage of the pulsed signal.

Wettability measurements provided the contact angle of the films in water. Contact angle values lie between 82 and 87°, which are higher than the data reported by Robertson (55–70°) [1]. This could be due to a decrease of the chemical affinity of the a-C:H with water, related to an aging effect during storage of the samples, which leads to passivation of the surface [13]. Furthermore, the contact angle seems to be independent of peak voltage. It has been reported that C–H bonds are hydrophobic, and different fractions of hydrogen for the prepared films were estimated by FT-IR [8]. However, the variation of hydrogen content in this case is not enough to produce changes in surface energy, so the deposition of hydrogen-richer samples is required to study the dependence of hydrogen abundance on wettability of a-C:H. Hysteresis is defined as the difference between contact angle in advancing and receding cycles. This parameter can be related to the roughness and the chemical heterogeneity of the surface [14]. In this case, hysteresis takes values between 20 and 30°, variations that are not important as expected for such smooth surfaces.

4. Conclusions

The growth characteristics of DLC films obtained by pulsed-dc plasma CVD technique, using methane as reactive gas, have been discussed as a function of plasma parameters. Differences between I–V characteristics and EEDF, at high- and low-power pulse level within a cycle, have been described and related to the corresponding plasma parameters, which explain the deposition rate behaviour of DLC films. An increase of electron temperature of approximately 1 eV is measured at high pulse level, and electron temperature and electron den-

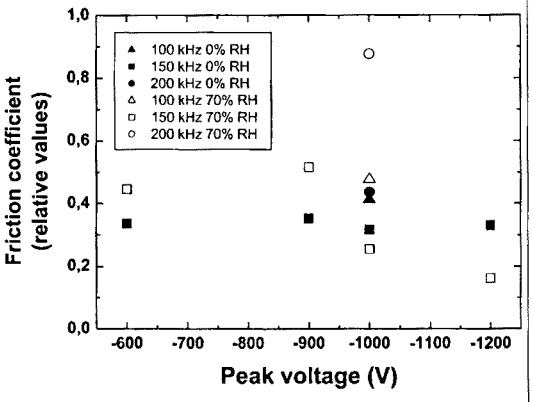

Fig 5 Evolution of the friction coefficient (in relative values) of a set of samples, evaluated at dry and moist conditions

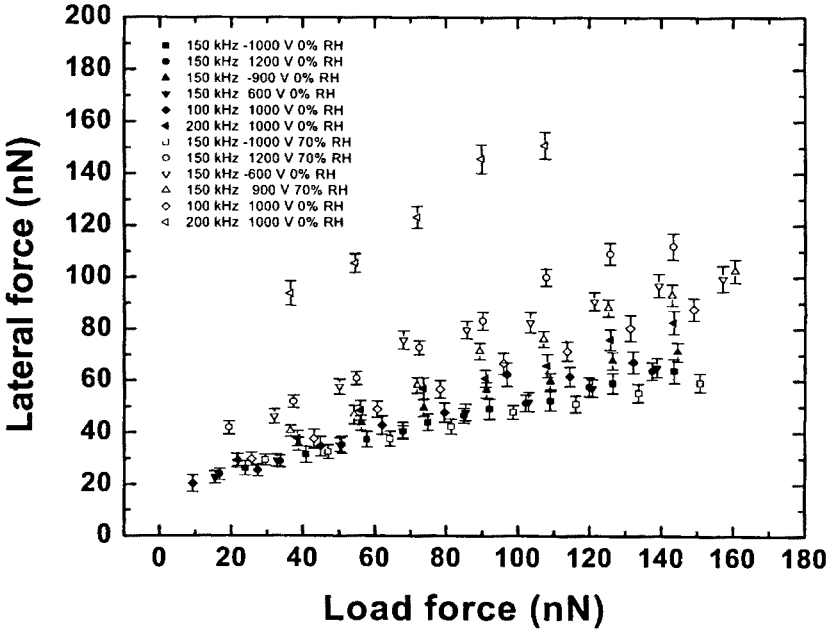

Fig 4 Plot of the lateral force vs. load force from a set of DLC films, obtained from AFM measurements in friction work mode under dry and moist conditions

sity go up with negative peak voltage, promoting DLC growth. The EEDF follow the Druyvestein equation and show plasma features at high- and low-pulse level. Film surfaces are smooth, and are found to roughen up to 1 nm at high bias voltage and low frequency, probably due to a greater atomic hydrogen etching. The dry nano-friction coefficient is not appreciably affected by preparation conditions. Contact angle measurements show that surface energy does not change with the deposition parameters.

Further investigation on methane plasma processes is needed in order to link deposition conditions with DLC film properties. A more accurate study, taking into account the variations of plasma parameters with more time-resolution measurements, and emphasizing their influence on DLC structure and mechanical properties, is planned

Acknowledgments

This work was supported by the CICYT of Spain (project MAT2002-04263-CO4 and MAT2003-02997) One of the authors (C.C.) acknowledges financial support of the Spanish MECD in the form of a FPU postgraduate scholarship.

References

[1] J Robertson Mater Sci Eng R 37 (2002) 129
[2] S R P Silva J D Carey, R U A Khan, L G Gerstner, J V Anguita in H S Nalwa (Ed), Handbook of Thin Materials, 4, Academic Press, 2002, p 403
[3] M Grischke, R Herb, O Massler, J Karner H Eberle, 44th Annual Technical Conference Proceedings Philadelphia, 2001
[4] I Michler M Grischke, I Traus K Bewilogua, H Dimigen, Diamond Relat Mater 7 (1998) 1333
[5] J-A Ruan, B Bhushan Trans Am Soc Mech Eng 116 (1994) 378
[6] FA Cali PA F Herbert WM Kelly, J Vac Sci Technol A 13 (1995) 2920
[7] J W Bradley, H Backer, PJ Kelly, R D Arnell, Surf Coat Technol 142-144 (2001) 337
[8] J I Andujar M Vives, C Corbella F Bertran, Diamond Relat Mater 12 (2003) 98
[9] C Hopf A von Keudell W Jacob Diamond Relat Mater 12 (2003) 85
[10] H Sugai, H Toyoda, J Vac Sci Technol A 10 (1992) 1193
[11] X L Peng, Z H Barber I W Clyne, Surf Coat Technol 138 (2001) 23
[12] V V Tsukruk, V N Blinzyuk, Langmuir 14 (1998) 446
[13] P B Leezenberg W H Johnston, G W Tyndall, J Appl Phys 89 (2001) 3498
[14] J-H Wang P M Claesson, J L Parker H Yasuda, Langmuir 10 (1994) 3887

4.6.2 Time-resolved electrical measurements of a pulsed-dc methane discharge used in diamond-like carbon films production.

C. Corbella[a,], M.C. Polo[a], G. Oncins[b], E. Pascual[a], J.L. Andújar[a], E. Bertran[a]*

[a]FEMAN, Departament de Física Aplicada i Òptica, Universitat de Barcelona, Av. Diagonal, 647, E08028 Barcelona, Spain

[b]Serveis Científico-Tècnics, Universitat de Barcelona, PCB, C/Josep Samitier, I-5 E08028 Barcelona, Spain

Thin Solid Films 482 (2005), 172-176

4.6.2.1 Summary

In this work, a series of DLC films were deposited on Si substrates by means of asymmetric bipolar pulsed-dc methane glow at different values of power frequency and amplitude voltage. Again, our contribution to this work was to assess the nanotribological properties of the resulting DLC films by means of LFM measurements. The same experimental setup as the one described in the previous section was used.

The conclusions concerning the nanotribological measurements can be summarized as follows:

- *The μ value for the obtained DLC films is proportional to the sample roughness. Then, variations of root mean square roughness (RMS) in the range 0.1 to 0.5 nm correspond with μ value variations from 0.2 to 0.32. If the RMS values had been more different, it could be proposed that the friction response is*

masked by the topography of the sample. Nevertheless, the roughness of the sample is extremely low in all cases, so we concluded that the nanotribological properties of the deposited films are not influenced by the sample topography and that the friction response depends on the deposition bias voltage value.

Available online at www.sciencedirect.com
SCIENCE DIRECT
Thin Solid Films 482 (2005) 132–136
thin solid films
www.elsevier.com/locate/tsf

Time-resolved electrical measurements of a pulsed-dc methane discharge used in diamond-like carbon films production

C. Corbella[a,*], M.C. Polo[a], G. Oncins[b], E. Pascual[a], J.L. Andújar[a], E. Bertran[a]

[a] *[illegible]*
[b] *[illegible]*

Available online 20 January 2005

Abstract

Amorphous hydrogenated carbon (a-C:H) thin films were obtained at room temperature via asymmetric bipolar pulsed-dc methane glow discharge. The power frequency values were varied from 100 to 200 kHz and the maximum amplitude voltage from −600 to −1400 V. Such films present diamond-like carbon (DLC) properties [J.L. Andújar, M. Vives, C. Corbella, E. Bertran, Diamond Relat. Mater. 12 (2003) 98]. The plasma powered by a pulse frequency of 100 kHz was electrically studied by a Langmuir probe. The next parameters were calculated within the pulse cycle from I–V measurements with 1 μs resolution: plasma and floating potentials, electron temperature and electron and ion densities. The presence of a population of hot electrons (10 eV) was detected at high bias voltage region. The density of cold electrons grows one order of magnitude after each negative pulse, whereas the ion density suffers a prompt increase during each positive pulse. The surface topography of DLC films was scanned by atomic force microscopy (AFM). A smoothly varying friction coefficient (between 0.2 and 0.3) was measured by AFM in contact mode. X-ray reflectivity (XRR) analysis provided a wide characterization of the films, involving density, thickness and roughness. The C:H ratio, directly obtained by elemental analysis (EA), shows an increase at higher bias voltages. All these features are discussed in terms of process parameters varied in film growth.
© 2004 Elsevier B.V. All rights reserved.

Keywords: Diamond-like carbon; Langmuir probe; Plasma parameters; Film characterization

1. Introduction

Diamond-like carbon (DLC) is a material whose physical and chemical properties have been extensively studied [2]. DLC is highly suitable for multiple applications when it is produced in thin film form. Most of the applications of this material take advantage of its excellent mechanical and tribological properties, and it is used mainly in protective coatings and solid lubricants. However, the high compressive stress achieved by these films limits their thickness tolerance below 1 μm. Research groups specialized in hard films have developed strategies to solve this disadvantage. Among these solutions is the incorporation of metal atoms in the carbon network via reactive sputtering physical vapour deposition (PVD). This leads to metal containing DLC films (Me-DLC) with a more relaxed structure [3,4]. The graded bias plasma-enhanced chemical vapour deposition (CVD) technique has also been successfully used, since the key parameter that controls the strains in the network is the bombardment energy of plasma species onto the film. More recent research has considered the use of pulsed high-power suppliers [5,6]. The main advantages of this technology are to reduce intrinsic stress, increase deposition rate and make production more cost effective.

The present article starts from previously reported research on DLC deposition by bipolar asymmetric pulsed-dc PECVD in methane environment [7]. The results discussed here are reported in two parts. First, we show and analyze the plasma parameters evaluated by a Langmuir probe. The inclusion of a time delay circuit to the experimental set reduced the resolution time to 1 μs for the electron temperature, the electron and ion densities, and the

* Corresponding author. Tel.: +34 93 403 79 92; fax: +34 93 402 11 35.
E-mail address: carles.corbella@uab.cat (C. Corbella).

0040-6090/$ - see front matter © 2004 Elsevier B.V. All rights reserved.
doi:10.1016/j.tsf.2004.11.135

plasma and floating potentials. Second, the surface properties of the films deposited in such conditions are presented. RMS surface roughness of the films is discussed as a function of the pulse frequency and the voltage amplitude. Nano-friction measurements were obtained through an atomic force microscopy (AFM) working-in-contact mode. More physical data were obtained by X-ray reflectivity (XRR) spectral analysis, whereas chemical composition was determined by elemental analysis (EA).

2. Experimental details

The DLC films were deposited on c-Si substrates placed on a water cooled cathode holder, by plasma CVD developed in a vacuum reactor provided with a load lock chamber and a computer-controlled gas supply and a pumping system. The process chamber was evacuated with a Roots pump coupled to a mechanical pump during the deposition process. Prior to each process the chamber was evacuated by a turbomolecular pump up to achieve a base pressure of 10^{-4} Pa. More details about the experimental set up are described in an earlier work [1]. A methane glow discharge was produced by powering the cathode-holder with an asymmetrical bipolar pulsed dc source (ENI RPG-50), operated between 100 and 200 kHz of pulse frequency. Methane gas was injected at a constant flow rate of 30 sccm as measured by a mass flow controller. The negative voltage amplitude ranged from −600 to −1400 V, whereas a constant positive pulse time of 2 μs was fixed to 40 V (Fig. 1), resulting in duty cycles from 80% to 60%. Some depositions were carried out by using rf power between −200 and −600 V of bias voltage. All the samples were processed at 10 Pa total pressure and room temperature.

The *I*–*V* characteristics from rf and 100 kHz dc discharges were recorded by means of an automatic Langmuir probe (SmartProbe model of Scientific Systems). The Langmuir probe was connected to a time-delay circuit to evaluate the *I*–*V* curves within one pulse cycle at a time resolution of 1 μs. A computer program processed the measured data and provided the plasma parameters, leading to an accurate tracking of the pulsed discharge throughout one period (10 μs). Prior to the Langmuir probe measurements, the chamber was cleaned by an oxygen plasma and the probe tip was cleaned in an argon rf discharge etching process as described elsewhere [8]. As regards the characterization of the deposited films, film thickness was obtained by means of surface profilometry using a Dektak 3030 instrument. XRR measurements were performed on a D-500 Siemens diffractometer equipped with a scintillation detector in high resolution operation mode using Bragg–Brentano geometry at a radiation wavelength of 0.154 nm. Surface topography was displayed using a multi-mode atomic force microscope with a Nanoscope IV electronics from Digital Instruments, which scanned 1×1 μm^2 areas in tapping mode at 2 Hz. Tribological properties in nanometric scale were evaluated by the same AFM operating in contact mode and calibrated for frictional forces measurements [9]. AFM scanned the films surface with a Si_3N_4 triangular cantilever of 100 nm tip radius at 1 Hz. The nominal tip radius was 10 nm, but it was abraded on mica in order to obtain a smoother tip surface. This was important in obtaining reproducible results [10] and a quasi-invariable tip radius during the experiments [9]. The AFM scanned transversally to the cantilever long axis in order to reduce hysteresis on piezoelectric actuators [11]. These measurements were performed in a dry atmosphere. The hydrogen-to-carbon ratio was provided by the detection of the oxidation products in a chromatographic column operation that was carried out in an EA 1108 CHNS-O Carlo Erba Instruments analyzer.

3. Results and discussion

3.1. Plasma diagnostics with a Langmuir probe

Fig. 1 shows the voltage signal waveform driven to the cathode by the pulsed-dc source in a methane discharge. Two regions are distinguished within the pulse: positive and negative, the latter being the most energetic. The plasma parameters corresponding to the 100 kHz methane discharge at −700, −900 and −1100 V of maximal amplitude were computed from the electrical current measurements performed by means of the Langmuir probe. A complete *I*–*V* characteristic was acquired each 1 μs, so a total of 10 curves were recorded per pulse cycle, the power evolution. These *I*–*V* characteristics were analyzed by fitting them to a two-temperature electrons model:

$$i_e = (\sqrt{\pi}/4)\, n_e \sqrt{\frac{8kT_e}{\pi m_e}} \left[i_e^{cold} \exp\left\{ \frac{e(V - V_s)}{kT_e^{cold}} \right\} + i_e^{hot} \exp\left\{ \frac{e(V - V_{pl})}{kT_e^{hot}} \right\} \right] \quad (1)$$

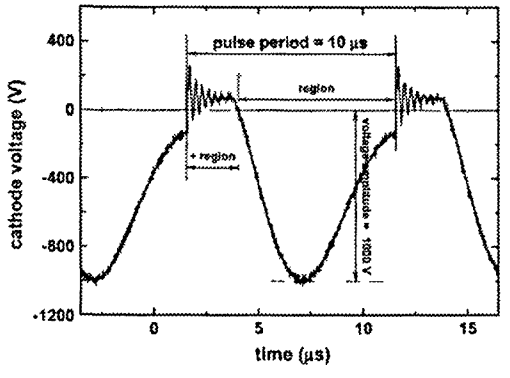

Fig. 1. Voltage signal waveform driven to the cathode by the pulsed-dc source in a methane discharge. Two regions are distinguished within the pulse: positive and negative, the latter the most energetic in all cases.

Here, i_e is the probe electron current; V is the probe bias, V_p is the plasma potential, identified as the maximum of the derivative of I–V curve; C is a constant; e is the elementary charge; k is the Boltzmann's constant; T_e^{cold} and T_e^{hot} are the temperatures of the cold and hot electrons populations, respectively; i_e^{cold} and i_e^{hot} are the cold and hot electron current contributions to plasma potential, respectively, which are related to the electron densities, n_e:

$$i_e = n_e e A \left(\frac{kT_e}{2\pi m}\right)^{1/2}. \quad (2)$$

where A is the probe area and m is the electron mass. The first term in Eq. (1) gives account of the ion current saturation regime. The constant C is approached to the magnetron conditions:

$$C = \frac{n_e A}{\pi}\sqrt{\frac{2e^3}{M}}. \quad (3)$$

From this approximation, we estimate the ion density, n_i. As hydrogen ion is the most immediately produced in methane discharge, we have approached ion mass, M, to the proton. The insets in Fig. 2 show an I–V measured characterisne along with the fit to the two-temperature model.

Fig. 2a–d collects the time evolution of plasma parameters within one cycle at a bias voltage of −900 V and are compared to those corresponding to rf discharges. For the positive region, the shortest in time, a single electron population of less than 1 eV temperature was measured. On the other hand, two electrons populations were detected in the negative bias voltage region, as in the case of de-sputtering magnetron plasma [12]. The coexistence of two electronic temperatures, as evidenced in the I–V plots from the insets in Fig. 2, takes place at the voltage bias inversion zone of the pulse cycle approximately 1 μs after the starting point of the negative pulse (Fig. 1). The temperature of the hot group achieves 10 eV and decays smoothly along the negative region, whereas the cold group keeps the temperature of the positive region. Another study [13] reported the formation of a single peak in electron temperature for an argon pulsed plasma in a magnetron system. However, this behaviour was not observed in our measurements, which is probably due to the absence of magnetron in the reactor. Indeed, a large number of hot electrons are able to reach the probe for a longer time because they are not trapped by any local magnetic field. This burst of hot electrons may arise from stochastic heating, mechanism that is promoted by the oscillation of the cathode sheath-edge [14]. The electron density during each pulse cycle is also divided into two groups (Fig. 2c). The density related to cold electrons increases over one order of magnitude after the positive bias region, reaching $6.5 \cdot 10^{10}$ cm^{-3}, whereas the corresponding

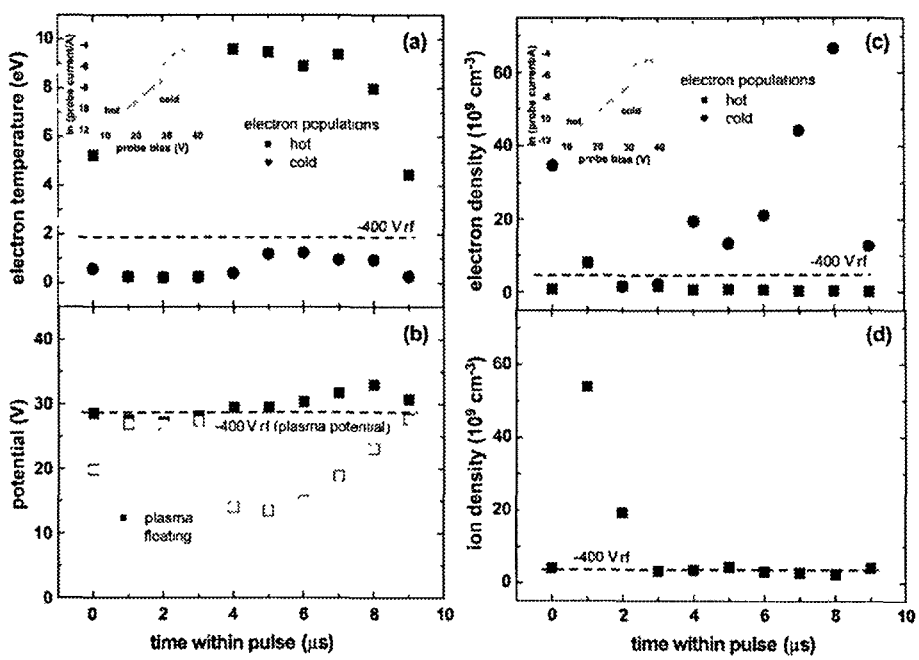

Fig. 2. Plasma parameters measured by a Langmuir probe within a cycle: electron temperature (a), plasma and floating potentials (b), electron density (c) and ion density (d). The dashed lines show the parameters corresponding to a rf discharge. The insets present the contribution from two electron populations.

to the hot electrons is almost constant. Electrons are confined in the plasma bulk during the discharge and they diffuse towards the reactor walls when plasma is switched off or weakened. This could be the reason for the electron depletion registered when bias is positive. Ion density shows a punctual growth in the positive region up to $5.5 \cdot 10^{10}$ cm^{-3}. Maximum values of ion and electron densities do not match the same time interval. Nevertheless, their respective values have the same order of magnitude. Hence, plasma quasi-neutrality is preserved over each pulse cycle.

Methane plasma potential achieves around 30 V in all bias values and varies very smoothly during the cycle, indicating that the plasma is not extinguished in the reversal bias period. This avoids cathode voltage spikes on the negative-going phase of the cycle and therefore arcing during the process. A different behaviour is shown by the floating potential, which follows a parallel evolution with the temperature of hot electrons. For the other studied bias voltages (−700 and −1100 V), plasma parameters present the same behaviour within each cycle. The plasma averaged parameters in one cycle are listed as a function of bias voltage in Table 1.

3.2. Analysis of the properties of DLC films

The RMS surface roughness from AFM scanning on surfaces of the DLC films is displayed in Fig. 3a. Scan area was 1×1 μm^2. For most of the depositions, a RMS roughness between 0.1 and 0.5 nm was measured. The overall tendency is the roughening of the surface as bias voltage increases until it reaches 1 nm RMS for DLC deposited at 100 kHz. A possible explanation was given in terms of surface etching by H atoms [7]. Fig. 3b shows the behaviour of friction coefficient, as measured by AFM in contact mode, against the bias voltage values. The friction coefficient was calculated from the linear fit analysis of the lateral force (friction) vs. the load force plot. The measured values range from 0.2 to 0.3. A lateral force is detected at zero load force in all the samples. This is attributed to a residual force of adhesion of the tip to the surface and varies between 0.5 and 2 nN. In general, a minimum of friction coefficient appears around −1000 V. Furthermore, the films prepared at 100 kHz of

Table 1
List of plasma averaged parameters measured in the pulsed dc methane glow discharge

Voltage amplitude (V)	Electron temperature (eV)	Electron density (10^9 cm^{-3})	Ion density (10^9 cm^{-3})	Plasma potential (V)	Floating potential (V)
−700	5.7–0.8	11–16.1	2.8	29.6	20.3
−900	5.6–0.6	15–22.4	10.9	29.6	21.3
−1100	5.8–0.5	17–22.8	7.7	30.7	19.3

The pulse frequency was 100 kHz. The values measured for the hot electron population precede the corresponding to the cold one.

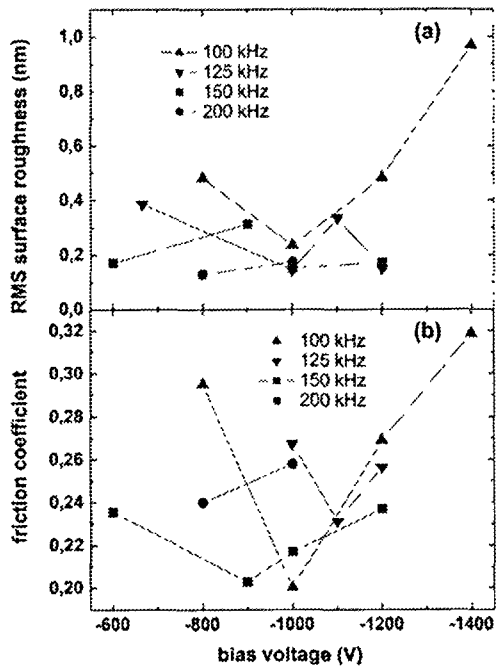

Fig. 3. RMS surface roughness (a) and friction coefficient (b) of DLC samples as a function of bias voltage during deposition. The measurements were carried out by AFM.

pulse frequency show a parallel evolution in friction coefficient and roughness. We also note the smoother variation of tribological properties when the preparation frequency increases, which is also a characteristic feature for surface roughness. In summary, at low frequencies, the bias voltage becomes a good control parameter for these surface properties.

The carbon-to-hydrogen ratio in the deposited DLC films has been evaluated by EA. The hydrogen content of DLC films deposited at higher bias voltages decreases with respect to less powerful discharges. Concretely, the DLC film deposited at −600 V contains approximately 60 at.% H, whereas for the sample prepared at −1400 V, a composition about 40 at.% H is detected. This evolution is consistent with qualitative measures of H content performed previously by Fourier-transform infrared spectroscopy (FTIR) [11]. When bias voltage increases, an enhancement of ionisation rate in the methane glow discharge appears. This leads to a stronger dissociation of methane molecules and, therefore, to a deposition of carbon-rich films [15].

The mass density of the films was derived from the critical angle for total external reflection of X-rays. The film thickness was determined by fitting the XRR spectra using the Fresnel equations and the results were in good agreement with those obtained by profilometry. Fig. 4a

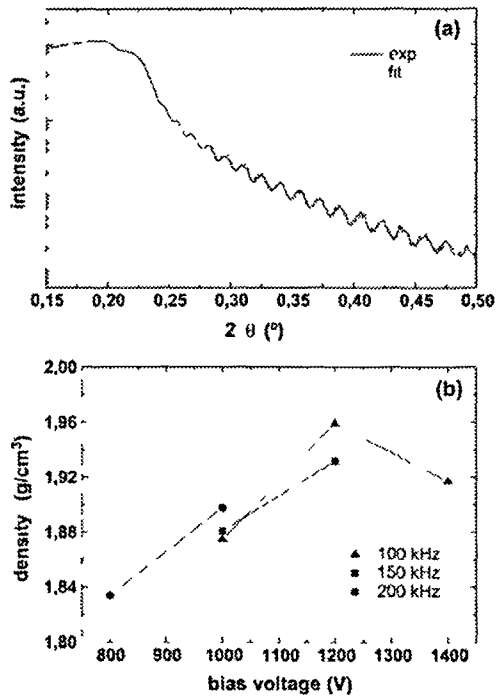

Fig. 4. XRR spectra (solid line) along with fitted curve (dashed line) (a) and mass density of DLC films vs. bias voltage (b).

shows a typical XRR curve for the deposited samples. Only one fringe period is seen, showing the absence of internal layering in the films. A double critical angle is clearly distinguishable. The lower angle corresponds to the hydrogenated carbon film and the second one corresponds to the silicon substrate, which means that the density of the films (between 1.8 and 2 g/cm³) is lower than that of the substrate (2.33 g/cm³). The density of the films increased in direct proportion with the bias voltage of the pulses for all frequencies tried (see Fig. 4b). This fact can be attributed either to the lower hydrogen incorporation in the films, which is consistent with EA results, or to a higher sp^3 fraction as the bias voltage increases. The sp^3 content in our films varies from 25 to 30%, using the relationship between sp^3 and mass density established by Tibassi et al. [16] comparing XRR and EELS measurements for ta-C and ta-C:H.

4. Conclusions

A pulsed-dc methane glow discharge was studied by Langmuir probe measurements. The coupling of a time-delay circuit facilitated an accurate monitoring of plasma parameters within a pulse of 100 kHz frequency. Two electron populations are distinguished in the negative region of the pulse. The hot group achieves 10 eV and has a stationary density, whereas the cold population presents an electron density that is one order of magnitude higher. Surface properties such as roughness and friction coefficient appear correlated and both show a dependence on bias voltage and pulse frequency. The dehydrogenation of DLC films as bias voltage increases is quantitatively confirmed by EA. The mass densities of the films, computed from XRR spectra analysis, are comprised between 1.8 and 2 g/cm³ and present a variation with the bias voltage that may be related to hydrogen content and sp^3 fraction. Hence, further studies are required on the structure of DLC films. More tribological and mechanical property measurements are planned in order to complete the characterization of these samples and link such properties with the film growth process per se.

Acknowledgments

This study was partially supported by the Generalitat de Catalunya (SGR 00078) and the CICYT of Spain (projects MAT 2002-04263-C04 and MAT 2003-02997). The authors thank Serveis Cientificotecnics of the Universitat de Barcelona for AFM, XRR and EA facilities. One of the authors (C. C.) acknowledges financial support of the DGU of the MICD for a postgraduate scholarship.

References

[1] H. Ando, M. Yoshikawa, T. Ogawa, E. Kamijo, A. Sawabe, Diamond Relat. Mater. 12 (2003) 96.
[2] J. Robertson, Mater. Sci. Eng., R Rep. 37 (2002) 129.
[3] H.D. Ingall, H. Habuchi, K. Morishita, Appl. Phys. Lett. 50 (1987) 1056.
[4] C. Corbella, M. Vives, A. Pinyol, E. Bertran, C. Canal, M.C. Polo, J.L. Andújar, Surf. Coat. Technol. 177–178 (2004) 269.
[5] T. Michler, M. Grischke, J. Fromm, K. Bewilogua, H. Dimigen, D. Leonhardt, Diamond Relat. Mater. 7 (1998) 459.
[6] E.H.A. Dekempeneer, J. Meneve, J. Smeets, Surf. Coat. Technol. 179 (1994) 1999) 647.
[7] C. Corbella, M. Vives, C. Pinyol, C. Canal, J.L. Andújar, E. Bertran, Diamond Relat. Mater. 13 (2004) 1695.
[8] J.A. Colligon, P.A.I. Hepburn, W.M. Kelly, J. Vac. Sci. Technol., A, Vac. Surf. Films 13 (6) (1995) 2920.
[9] D.O. Jones, R.W. Carpick, M. Salmeron, Rev. Sci. Instrum. 67 (1996) 3238.
[10] L. Qian, X. Xiao, S. Wei, Tribol. Int. 36 (2003) 663.
[11] J.-A. Kuo, B. Bhushan, Trans. Am. Soc. Mech. Eng. 116 (1994) 389.
[12] H. Sternberg, M.J. Goeckner, J. Vac. Sci. Technol., A, Vac. Surf. Films 9 (3) (1991) 688.
[13] J.W. Bradley, H. Backer, P.J. Kelly, R.D. Arnell, Surf. Coat. Technol. 135 (2001) 221.
[14] D.A. Glocker, J. Vac. Sci. Technol., A, Vac. Surf. Films 11 (6) (1993) 2989.
[15] A. Hart, B. Dwyer, Thin Solid Films 258 (2000) 86.
[16] A. Tibassi, A.C. Ferrari, S. Silva, B.K. Tanner, J. Robertson, L.M. Brown, Diamond Relat. Mater. 9 (2000) 771.

4.6.3 Mechanical Properties of Alkanethiol Monolayers studied by Force Spectroscopy

G. Oncins[a], *C. Vericat*[a,b], *F.Sanz*[a]

[a]Institut de Bioenginyeria de Catalunya (IBEC) and Department of Physical Chemistry, Chemistry Faculty, University of Barcelona, Martí i Franquès 1-11, 08028, Barcelona (Spain)

[b]Instituto de Investigaciones Fisicoquímicas Teóricas y Aplicadas (INIFTA), La Plata, Argentina

Submitted to Journal of Chemical Physics

4.6.3.1 Summary

The nanotribological properties of alkanethiol monolayers have been extensively studied in the past and they have proved to be really good lubricant films. Nevertheless, it remains unclear which is the deformation process that these monolayers undergo when they are compressed vertically, that is, when they are nanoindented. One of the first experimental studies in this field was performed by Barrena et al.[218], who proposed a model for alkanethiol deformation that consisted in a cooperative tilting of the monolayer as a response to external pressure. The striking idea was that the molecular tilting angles are discrete values because the tilting process is governed by the van der Waals interactions between the chains, which only interlock at certain angles. Other authors proposed that the energy to create gauche defects in the terminal ends of the hydrocarbon chains was in the range of energies that an AFM tip could provide during the scanning process and that the cooperative tilting model required too much energy. In this work, we performed Δx vs. Δz and F_v vs. P_d curves on decanethiol and hexadecanethiol

monolayers on monocrystalline Au(111) and studied the compression process, reaching these conclusions:

- *During Force Spectroscopy experiments, the monolayers are penetrated in a discrete way, that is, the monolayer thickness do not decrease linearly with pressure but in a step-by-step sequence. The step thickness can be experimentally measured but it could correspond both to the creation of a terminal gauche defect or to the first allowed molecular tilting.*

- *The F_v value to trigger the first folding event highly depends on the compactness of the monolayer. Experimental pressure calculations suggest that the first folding event in compact monolayers is due to a cooperative molecular tilting, while the creation of gauche defects is more plausible for non-compact monolayers.*

- *The Young's modulus was calculated for these monolayers applying a recently developed model, obtaining values in the range of 50-150Pa.*

Mechanical Properties of Alkanethiol Monolayers studied by Force Spectroscopy

Gerard Oncins

Institut de Bioenginyeria de Catalunya (IBEC) and

Department of Physical Chemistry, Chemistry Faculty, University of Barcelona, Martí i Franquès 1-11, 08028, Barcelona (Spain)

Carolina Vericat

Institut de Bioenginyeria de Catalunya (IBEC),

Department of Physical Chemistry, Chemistry Faculty, University of Barcelona, Martí i Franquès 1-11, 08028, Barcelona, Spain and

present address: Instituto de Investigaciones Fisicoquímicas Teóricas y Aplicadas (INIFTA), La Plata, Argentina

Fausto Sanz

Institut de Bioenginyeria de Catalunya (IBEC) and

Physical Chemistry Department, Chemistry faculty, University of Barcelona, Martí i Franquès 1-11, 08028, Barcelona, Spain

Abstract

The mechanical properties of alkanethiol monolayers on Au(111) in KOH solution have been studied by Force Spectroscopy. The analysis of the vertical force vs. penetration curves showed that monolayer penetration is a stepped process that combines elastic regions with sudden penetration events. The structural meaning of these events can be explained both by the creation of gauche defects on the hydrocarbon chains and by a cooperative molecular tilting model proposed by Barrena et al in ref. 24. The validity of these models for alkanethiol monolayers of different compactness and chain length has been discussed. The Young's modulus (E) of the monolayers has been calculated by using a recently developed model which considers the thickness of the monolayer as a parameter, thus allowing a decoupling of the mechanical properties of the thiols layer from those of the Au(111) substrate. As a result, the calculated E values are in the range of 50-150Pa, remarkably lower than those previously reported in the literature.

Introduction

Self-assembled monolayers (SAMs) have been a matter of extensive research during the last decades. The development of micro and nanofabrication techniques and the need to find durable lubricants at the molecular level for MEMS and NEMS have been some of the most important applications of these monolayers[1-3]. Since alkanethiol SAMs on gold were prepared for the first time, several aspects concerning their chemical and physical properties have been studied[4]. Their structure has been resolved using different spectroscopic techniques[5-7] and Scanning Probe Microscopies (SPM)[8]. Thiol molecules arrange in ordered lattices, the most usual being the $(\sqrt{3}\times\sqrt{3})R30°$ lattice and its related c(4×2) superlattices[9-11]. The hydrocarbon chains generally adopt an all-trans configuration, although gauche defects at the end of the molecule opposite to the S head are usually found at room temperature[5,12]. Poirier[13,14] performed Scanning Tunneling Microscopy to resolve the different phase transitions that decanethiol molecules undergo as they assemble on Au(111) in ultra high vacuum conditions. Xu et al.[15] followed the in-situ self- assembly of alkanethiol molecules in liquid environment by Atomic Force Microscopy (AFM) and proposed a mechanistic model for the process.

Several Density Functional Theory (DFT) studies and Molecular Dynamics (MD) simulations have been performed to establish the bonding site of the thiol on Au and the tilt angle (θ) between the alkanethiol molecule and the Au surface normal[16-19], though some controversy still exists between theory and experiment concerning the preferred adsorption site[20]. As regards the study of thiol monolayer mechanics, Joyce et al.[21] used the Interfacial Force Microscopy (IFM) to compress a hexadecanethiol monolayer, detecting a mechanical hysteresis that was related to a wholly inelastic behavior. Molecular Dynamics[22] and Monte Carlo simulation[23] studies proposed that the tilting of the molecules with respect to the Au surface and the creation of gauche defects on the terminal methyl groups of the hydrocarbon chains played a key role in the monolayer deformation process under pressure. In AFM studies of alkanethiol islands in air by Ocal et al.[24-26], it was observed that the height of the monolayer decreased as the vertical force was increased, and thus the authors proposed that thiol molecules tilted in quantized angles to maximize the Van der Waals interactions between the hydrocarbon chains. Recent experimental studies concerning the analysis of Ultrafast Dynamics of Shock Compression[27] and Vibrational Spectroscopy[28] suggested that the structural mechanism to accommodate compressive vertical forces depends on the length of the hydrocarbon chain and also on the defect density of the monolayers.

The aim of the present work is to study the mechanics of decanethiol (DT) and hexadecanethiol (HDT) monolayers deposited on Au(111) surfaces in liquid environment by means of Force Spectroscopy, technique that is widely used to quantify surface forces[29]. Measurements of alkanethiol SAMs on gold in aqueous electrolytic solutions are important because some of their most important applications, like biosensing and bio- recognition and corrosion protection, involve such media. Although these SAMs have been much studied, some aspects of the mechanisms involved in charge transfer and the importance of defects and other heterogeneities in the monolayers are still a matter of debate. Alkaline solutions (KOH and NaOH) are the electrolytes of choice for electrochemical measurements and for Scanning Tunneling Microscopy and Scanning Tunneling Spectroscopy in liquid environment, either under electrochemical control or not, because they provide the wider stability range and allow a complete controlled electrodesorption of the SAMs[30]. Our group has recently performed electrochemical STS measurements of alkanethiol SAMs on Au(111) in 0.1 M KOH and has found some interesting results. From current- potential curves, changes

in conductance that cannot be related to thiol electrodesorption were found that could be attributed to changes in the layer permeation. On the other hand, current- distance curves - which involve approaching and retracting an Apiezon- covered STM tip - show two slopes, which can be related to the STM tip inside and outside the thiol SAM[31].

This paper is the first step to study alkanethiol SAM mechanical properties in the electrolyte of interest for electrochemical STS, to try to separately understand the electronic and mechanical aspects involved in electrolytic/SAM interfaces before performing more complicated combined experiments that involve AFM measurements under electrochemical control.

Several studies using Force Spectroscopy have been performed in our laboratory, especially to test the mechanical properties of phospholipid bilayers in aqueous solution[32,33]. In the present work, we show that alkanethiol monolayers can be compressed in a quantized way, and that the thickness of these penetration events can be measured and related to structural changes in the monolayer. Moreover, it will be seen that the vertical force needed to penetrate the monolayer is highly dependent on its compactness and that the total penetration changes with the length of the hydrocarbon chain, i. e., the monolayer thickness. Thanks to a recently developed approach to calculate elastic constants of soft layers on hard substrates[34,35], the Young's modulus of DT and HDT monolayers have been calculated.

Experimental Section

Materials

1-decanethiol (DT, 96% w/w; from Aldrich) and hexadecanethiol (HDT, >95% w/w; from Fluka) were used without any further purification. Analysis-grade ethanol (99.9%; from Carlo Erba) was used for the thiol solutions. Water was purified by distillation followed by deionization in an ion-exchange unit and then passage through a Milli-Q RG system consisting of charcoal filters, ion exchange media and a 0.2μm filter. Au(111) single crystals were obtained from MaTeck (Juelich, Germany).

Sample preparation

The Au(111) single crystals were electropolished at +10 V in 0.1M H_2SO_4 for 30 sec, rinsed with Milli Q water and immersed in 1M HCl for 10min to remove the thick oxide layer. After thoroughly rinsing with Milli-Q water and drying with Ar, the crystals were annealed in a butane flame (3min) and gently cooled under Ar flow for 2min. This process yields clean Au(111) surfaces with terraces about 1μm wide, as topographically checked by AFM. Just after surface preparation, the gold samples were immersed in 0.05mM DT or HDT ethanolic solutions for 24-72hs. After that, the samples were rinsed with ethanol, dried with a N_2 gas flow and glued on Teflon discs with adhesive film. The samples were covered with 50-70μl (a big droplet) of 0.1M KOH solution.

AFM measurements

All experiments were performed in a Dimension 3100 atomic force microscope attached to a Nanoscope IV electronic controller (Digital Instruments, Santa Barbara, CA) under controlled temperature (20-22°C). Silicon nitride V-shaped tips with a nominal spring constant of 0.5N/m were used for imaging and for force spectroscopy measurements (MLCT-AUNM microlever probes, Veeco, Santa Barbara, CA). After the force spectroscopy experiments, cantilevers were individually calibrated in an Asylum 3D atomic force microscope (Asylum Research, Santa Barbara, CA) with the thermal noise method[36] and the cantilever sensitivity as calculated (V/nm) by performing force curves on a hard substrate for several minutes to avoid piezo drift.

Before performing the force spectroscopy experiments, the Si_3N_4 tip was immersed in the KOH solution droplet for 15 minutes to equilibrate temperatures. The tip radius was measured before and after the experiments by imaging sharp silicon oxide ridges (Ultrasharp TGG01 calibration grating. Mikromasch, Tallinn, Estonia) and no tip etching effects due to the medium were detected. All force experiments were performed at 0.15-0.25 μm/s to avoid any influence of the indentation velocity on the monolayer penetration process. Applied vertical forces, F, are given by $F = k_c \times \Delta$, where Δ is the cantilever deflection and k_c is the cantilever spring constant. The surface deformation is given as penetration $\delta = z - \Delta$, where z represents the piezo-scanner displacement. X-,

Y- and Z- piezo motion was calibrated with a Digital Instruments silicon oxide grid (STR10-1800P), 180nm deep, 10μm pitch.

Results and Discussion

Force spectroscopy measurements

Prior to performing force curves, the thiol-covered Au(111) surface was imaged in contact mode to ensure that the force spectroscopy study would be performed on clean areas with no substrate defects (steps, dislocations, etc) (Fig.1a). As it can be seen in the image and in the section profile, there are regions of different height within a given terrace due to the existence of disordered, flat-lying and missing molecules[37] mixed with the compact monolayer. The presence of these kinds of defects has been reported in previous AFM studies of the structure and the adsorption kinetics of alkanethiol SAMs on Au(111)[38,39].

Fig.1b shows a vertical force vs. penetration curve ($Fv\delta$) on a DT SAM on Au(111). The response of a freshly annealed, bare Au(111) surface and the effect of spurious contamination on $Fv\delta$ curves were also checked (See Supporting Information figure I). In this work, the contact point between tip and sample is considered as penetration 0nm, so the negative penetration region in the $Fv\delta$ curves corresponds to the non-contact region between the tip and the surface. In the non-contact region prior to the contact is where the effect of the Electric Double Layer (EDL)[40] can be quantified. Nevertheless, although the Si_3N_4 tip is charged[41,42] at the pH of the experiment, the sample surface is not charged (methyl terminal groups), so electrostatic interaction is considered negligible in the interpretation of the $Fv\delta$ curves. After reaching the contact point (penetration 0nm), the tip compresses the monolayer (region 1 in the inset). This compression yields a linear relationship between F and δ, with a positive slope. Then, there is a sudden penetration with a negative slope (from now on called "sudden penetration event" and marked with a *), which represents an abrupt decrease of the monolayer thickness. Next, a region in which the monolayer is compressed appears again (region 2 in the inset), followed by another sudden penetration event (also marked with a *). Finally, the monolayer is further compressed (region 3 in the inset,) until

there is no more penetration (hard contact region). Force curves on HDT show a similar behavior.

The δ values shown in this work were considered as the penetration increment from the contact point between tip and sample to the hard contact region (infinite slope in the $Fv\delta$ curve). Then, δ values can be used as sample thickness control checks to ensure that there is no contamination on the alkanethiol samples. The histograms in Fig.2 show an analysis of δ values measured in $Fv\delta$ curves for DT (Fig.2a) and HDT (Fig.2b). The measurements were performed in at least 5 different points of each sample and by recording approximately 50 force curves per point. These conditions apply for all the samples analyzed in the present work. The gaussian fittings yield total penetrations of 15.3±3.2Å and 26.4±5.1Å for DT and HDT, respectively, in agreement with the thicknesses calculated with ChemDrawPro (CambridgeSoft, MA) for DT and HDT monolayers tilted 35°, which are 15.0 and 22.6Å.

Fig.2c and 2d show the calculated penetration value of the sudden penetration events (δ_p), marked with a * in Fig.1. Interestingly, δ_p gaussian fitting shows a peak at 1.9±1.3Å for DT and at 2.2±2.0Å for HDT. The concordance between δ_p for the two different length monolayers suggests that the folding process is the same regardless of the length of the hydrocarbon chain.

In order to understand the structural changes undergone by the samples during the compression, the number of sudden penetration events for each $Fv\delta$ curve was calculated. After testing different samples (and different regions in each sample), it can be concluded that DT monolayers show a mean value of 2.66±1.11 events per $Fv\delta$ curve, while HDT monolayers show 2.94±0.97 events. These aspects will be considered in more detail in the *Folding Mechanism* section.

Although most of the thiol-covered Au(111) surfaces presented structural defects (as seen in Fig.1a), some islands were found to have a more compact structure, as the one shown in Fig.3a. The presence of compact domains had been previously detected by AFM in mechanical studies of alkanethiols in air[43-45] and we have detected them in DT monolayers but not in HDT samples. Interestingly, the mechanical response of these compact regions is characteristic as it can be seen in the $Fv\delta$ curve depicted in Fig.3b. After contact (penetration 0nm), there is a linear compression region until a vertical

force of 3nN is reached (similar to region 1 in Fig.1b). Then, there is a sudden penetration event similar to those seen in non-compact alkanethiol monolayers (Fig.1b, here also marked with a *) that corresponds to the penetration of a DT monolayer. According to this, two points must be considered: (a) in compact domains F to trigger the monolayer penetration goes from 1-4nN, depending on the sample and on each particular island, (b) this force ranges from 50-100pN for non-compact alkanethiol monolayers. This fact points out that the compactness of the monolayer plays a key role in the mechanical properties of the surface under compression[46]. The second point is that in compact domains the thickness decrease occurs at a certain F, while in the less compact areas individual sudden penetration events can be clearly discriminated (Fig.1b). Nevertheless, in the inset of Fig.3b it can be seen that the unique folding event in compact domains is probably composed of several sudden penetration events (as in non-compact monolayers). Unfortunately, because of the resolution limitations of the performed $Fv\delta$ curves, it was not possible to calculate the mean penetration value for each of these events.

Young's modulus

Young's modulus, E, is a mechanical parameter widely used to study the elastic properties of materials. E can be expressed as

$$E = \frac{\left(\frac{L_0}{\Delta L}\right)}{\frac{F}{A}} \qquad (1)$$

Where L_o is the initial length of the material, ΔL represents the extension or compression of the material and A is the area of contact. Being an elastic constant, E can only be calculated as long as the elastic limit of the material is not surpassed, that is, before any plastic deformation.

Several attempts have been done to calculate E for thiol monolayers, although the discrepancies in the values of E between the different applied methods are remarkable. In fact, simulation studies[47,48] rendered E values of 20±10GPa, irrespective of the hydrocarbon chain length. A recent experimental study[49] used the change in the

resonant frequency of the tip[50,51] due to the proximity of the sample to calculate the mechanical properties of alkanethiol islands of different size, concluding that E strongly depends on the size of the alkanethiol islands and giving values around 1GPa. Force spectroscopy measurements were also performed by Domke et al.[52], who tested the mechanical properties of thin films and applied Hertz[53]-Sneddon[54] contact mechanics, a modification of Hertz theory that models the contact between a cone and a flat surface. In this model, F is expressed as

$$F = \left(\frac{2}{\pi}\right)\left[\frac{E}{\left(1-\nu^2\right)}\right]\delta^2 \tan(\alpha) \qquad (2)$$

where ν is the Poisson ratio of the sample, δ is the indentation depth and α is the half opening angle of the tip cone. The analysis of polymeric thin films using Hertz-Sneddon model rendered values of E that strongly depended on the film thicknesses: as the film thickness decreased, E increased in a non linear way. It was then concluded that the E values obtained with this model (in the range of kPa) were significantly influenced by the mechanical properties of the substrate underneath the film, and that they were an upper limit for the real value of the Young's modulus. Nevertheless, this model is really useful to calculate the mechanical properties of structures wider than ~1μm, as is the case of living cells[55].

In our case, as a (soft) organic monolayer is deposited on a hard substrate, the Hertz-Sneddon, DMT and JKR contact mechanics models would lead to monolayer E values strongly influenced by the substrate. To overcome this limitation, a different model that has been recently proposed by Dimitriadis et al.[56] was applied. For a monolayer bonded to the substrate,

$$F = \left(\frac{2\pi}{3h^3}\right)ER^2\delta^3 \qquad (3)$$

where R is the probe radius and h is the sample thickness. As h is taken into account, the mechanical properties of the substrate and the monolayer can be decoupled and more reliable monolayer E values are obtained. This expression is valid for samples bonded to the substrate and for $h<0.1R$ and assumes a $\nu = 0.5$, which is in agreement with the value calculated by Beach et al.[57] for HDT monolayers on Au. The model proposed by Dimitriadis has been used to calculate the elastic properties of purple

membranes while varying the salt concentration of the medium performing force spectroscopy measurements[58].

In the present study, E was calculated for non-compact DT and HDT monolayers and for compact DT domains. We have compared the results obtained by using both the Sneddon-Hertz (equation 2) and the Dimitriadis (equation 3) models. It is important to note that Sneddon-Hertz model approximates the tip to a cone, so it is a simplification of the real shape of the tip apex. Consequently, the obtained results have to be regarded as qualitative and just as a reference to compare with the Dimitriadis model. Since E is an elastic property of the monolayer, it has to be calculated in the elastic regions of the $Fv\delta$ curve. As it has been previously shown, alkanethiol monolayers under compression show an initial elastic region followed by a sudden penetration event. This process can be repeated 1-4 times as the monolayer thickness decreases. Then there is another elastic region as the monolayer is further compressed and finally we find a hard contact between the sample and the tip. Fig.4 shows a $Fv\delta$ curve obtained on a "non-compact" DT monolayer. This curve is equivalent to Fig.1b, although this individual curve shows four sudden penetration events. Two different E values were calculated for each $Fv\delta$ curve, considering the elastic regions marked as "initial" and "final" in Fig.4. It has not been possible to calculate E for all the intermediate elastic regions prior to a penetration event because of the $Fv\delta$ resolution. For the Sneddon-Hertz model calculations E values were obtained from the slopes of the corresponding elastic region in the $Fv\delta^2$ curves. The half opening probe angle (α) was calculated by scanning a calibration grating with sharp silicon oxide ridges (Ultrasharp TGG01. Mikromasch, Tallinn, Estonia). For the Dimitriadis model calculations, E was obtained from the slopes of the corresponding elastic region in the $Fv\delta^3$ curve. This model modifies Hertz-Sneddon theory by taking the monolayer thickness (h) into account. Since h changes as the penetration events take place, it is different in the initial and final elastic regions. We have assumed that the region of hard contact between the tip and the monolayer corresponds to a monolayer height of 0.4nm, which is the diameter of an alkyl chain. This situation corresponds to the monolayer fully compressed against the Au surface. In Fig.4, h_i and h_f represent the h values for the initial and final elastic regions respectively, although it is necessary to add 0.4nm to h_i and h_f to account for the total height of the monolayer in each compression state.

Table 1 shows the obtained E values using Hertz-Sneddon and Dimitriadis models. The differences in the calculated values between the two methods are remarkable. As expected, E values obtained from Hertz-Sneddon calculations are higher than those obtained with the Dimitriadis model. This fact is in agreement with the calculations performed by Domke[59], who concluded that Hertz-Sneddon model is sensitive to the substrate E when the film is extremely thin, which is the case for alkanethiol monolayers. Interestingly, the Hertz-Sneddon model renders higher E values for the final elastic region than for the initial elastic region. As seen in Fig.4, the slopes of the consecutive elastic regions in $Fv\delta$ curves increase as δ increases. In conclusion, the results from the Hertz-Sneddon model would lead us to conclude that the monolayer progressively hardens as the sudden penetration events take place. On the other hand, Dimitriadis considers not only the slope of the $Fv\delta^3$ curve elastic regions, but also h^3. As the slopes of the elastic regions increase (more penetration events have taken place), h decreases. These two factors balance each other, rendering a similar E value for the initial and for the final elastic regions.

No significant differences were seen between E values for DT, compact DT and HDT monolayers. The nature of the E calculations presented in this work is semi-quantitative, mainly because of the error introduced in the calculation of h in each $Fv\delta$ curve. Further work will be done to refine the presented results and to clarify if different length and compactness in the thiol monolayers yield different E values. Nevertheless, from our results and by considering the Dimitriadis model, the E values for alkanethiol monolayers range from 50 to 150Pa. These values are much lower than the values found in the literature (in the range of the GPa for simulation studies[48,60]; around 1GPa for more recent experimental measurements[61]), which were influenced by the underlying substrate. The results we present in this work are direct experimental measurements that involve the intimate contact between the tip and the thiol monolayer. Very specific instrumental conditions were needed to detect the sudden penetration events shown in $Fv\delta$ curves, such as force curves with a z piezo movement around 50nm. In addition, full compression of the monolayers involved vertical forces in the pN range (only the DT monolayer showed penetration events in the nN range). All these facts lead us to think that information about the mechanical properties of alkanethiol monolayers can be easily masked by the properties of the substrate and that a very sensitive technique as

force spectroscopy is necessary to accurately calculate the elastic properties of these materials.

Folding mechanism

Two different mechanisms have been proposed in the past to explain the monolayer deformation as F is applied: the creation of gauche defects in the hydrocarbon chains and the cooperative tilting of the whole alkanethiol molecule, models that have been reviewed by Salmeron et al.[62] Cooperative tilting under pressure was proposed by Barrena et al.[63-65] after studying alkanethiol compact islands deposited on Au(111) and imaged with AFM in air. Molecular dynamics simulations[66] have been performed to explain interface force microscopy compression experiments on a similar basis[67]. In this model (depicted in Fig.5a) it is proposed that alkanethiol molecules undergo quantized tilting events when compressed, so that the resulting tilting angles (θ) maximize van der Waals interactions between the hydrocarbon chains. The model was then improved by maximizing the chains interlocking in 2D[68], obtaining good agreement with the experimental results. Table I in Supporting Information shows the theoretical thicknesses for HDT and DT monolayers when the cooperative tilting model is applied. It is assumed that θ is 35° when no pressure is applied on alkanethiol monolayers[5]. Interestingly, the calculated values for thickness diminution between consecutive permitted tilting angles are ≈2Å for both DT and HDT, in agreement with the value we have experimentally measured for the sudden penetration events shown in Fig.2. However, in the case of the works by Barrena et al., the cooperative tilting process was proposed for small and compact alkanethiol islands whose thicknesses were calculated as the tip scanned the surface. Our measurements were performed mostly on non-compact alkanethiol monolayers (Fig.1a) and the sample was not scanned but punctured, so a cooperative tilting process seems to be less likely to happen when there are defects in the layers. The presence of defects can be attributed to the liquid environment, as it was studied in the past by means of Infrared techniques. It was concluded that terminal disorder in the alkyl chains was induced by the solvent, in that case D_2O, CD_3OD and CCl_4[69] In this line, a recent work studied the in-situ effect of ethanol on the molecular arrangement of the alkanethiol chains, concluding that a long range disorder is observed after adding the solvent and that the initial ordered structure

can be recovered drying the sample with helium[70]. By all this, the sample surrounding media plays a key role in the structural and mechanical properties of the alkanethiol monolayers.

Another way to dissipate the energy applied by the tip on the monolayer is the creation of gauche defects in the hydrocarbon chain (Fig.5b)[71-74]. Table II in Supporting Information shows the height of DT and HDT molecules as gauche defects are introduced in the chain. Hyperchem software (HyperCube Inc., Gainesville, FL) was used to constrain certain bond torsion angles to +60 or -60°. Thickness diminution introduced by each gauche defect is ca. 2Å. Thus, the sudden penetration events in our $Fv\delta$ curves can be explained both by the alkanethiol molecular tilting and by gauche defects creation.

It has been proposed that the energy needed to create gauche defects in the core of a hydrocarbon chain is too high to be considered a reasonable process[75] because of the stabilizing van der Waals forces exerted by the surrounding hydrocarbon chains. Nevertheless, the energy to create a single gauche defect in the terminal carbon of an alkane chain is relatively low (2.9kJ/mol)[5,76]. Moreover, both molecular dynamics simulations[77,78] and experimental AFM measurements[79] support the fact that the number of terminal gauche defects increases rapidly during the first compression stages. Interestingly, the presence of a second gauche defect in alkanethiol monolayers under pressure has been also experimentally detected by means of Ultrafast Dynamics of Shock Compression[80].

The energy exerted by the tip on the monolayer is $E = F^* \delta$. To prove if the energy necessary to trigger the first penetration event observed in $Fv\delta$ curves is consistent with the energy needed to create a terminal gauche defect, we first attempted to apply the contact mechanics model proposed by Hertz[81]. Unfortunately, Hertz model does not consider the case in which there is a soft monolayer on a hard substrate and the calculated contact area would have been meaningless. Instead, a simple geometric model was applied. As seen in Fig.2c and 2d, sudden penetration events result in a monolayer height diminution of ≈0.2nm. Nevertheless, to calculate δ, also the initial elastic region (Fig.4) has to be considered, rendering δ = 0.5nm for the elastic region plus a sudden penetration event. To calculate the number of molecules affected by the tip as it penetrates 0.5nm in the monolayer, we have considered the tip to be an

uncompressible sphere of radius *R*. Then, the maximum contact area between tip and sample is the area of a 0.5nm height spherical cap. This simple model was used to calculate the experimental pressure values reported in this work. The calculated energy of the process is 4.0kJ/mol if an area per molecule of 21.4Å[22] is considered (compact monolayer) and 5.8kJ/mol if a 30% of vacancies are included[82]. These values are comparable with the 2.9kJ/mol necessary to create a terminal gauche defect[83].

The calculated pressure exerted on a non-compact monolayer to trigger the first sudden penetration event is 63MPa. AFM and nonlinear optical experiments performed on alkanethiol and alkanesilane monolayers showed that pressures smaller than 80MPa are enough to create terminal gauche defects[84-86]. On the other side, Barrena reported that the pressure to trigger the first alkanethiol chain tilting is much higher (0.5GPa)[87]. In conclusion, it is plausible to consider that the first sudden penetration event seen in $Fv\delta$ curves in the non-compact monolayers corresponds to the creation of terminal gauche defects.

For the compact DT domains ($Fv\delta$ curve shown in Fig.3b), the pressure exerted on the monolayer to trigger a sudden penetration event ranges from 1.2 to 4.2GPa. This value suggests that, in this case, the first sudden penetration event can also be due to a cooperative molecular tilting.

To conclude, vertical forces at which the first sudden penetration event takes place are remarkably different for compact (vertical forces 1-4nN) and non-compact (vertical forces 50-100pN) alkanethiol monolayers. This fact proves the importance of packing density in the mechanics of alkanethiol monolayers. In fact, the presence of vacancies lets the monolayer dissipate the applied compression energy and it is necessary not only to create gauche defects but also to trigger cooperative molecular tiltings[88]. As it has been said before, there are 2-4 sudden penetration events per penetration curve for all studied monolayers, so deformation mechanisms for compact and non-compact monolayers can be different combinations of gauche defects creation and cooperative molecular tiltings. The calculation of the pressure exerted on the monolayers suggests that the creation of gauche defects is the main energy dissipation mechanism in non-compact monolayers, while cooperative molecular tilting could be the preferred mechanism in compact alkanethiol domains.

Conclusions

DT and HDT monolayers deposited on Au(111) single crystals have been studied by force spectroscopy in KOH solutions. The analysis of the *F*vs*δ* curves showed the presence of sudden penetration events as the monolayer was punctured by the AFM tip. The monolayer thickness diminution corresponding to the sudden penetration events was calculated (ca. 2Å) and related to the creation of gauche defects and cooperative molecular tilting. The pressures needed to trigger the first sudden penetration event in non-compact monolayers (≈63MPa) suggest that this process corresponds to the creation of gauche defects. However, the pressure is much higher in compact domains (1.2 to 4.2GPa), so we propose that in this case a cooperative molecular tilting is responsible for the first sudden penetration event. Calculated pressures are in good accordance with the literature[89].

The Young's modulus of the alkanethiol monolayers was also calculated, rendering values ranging from 50 to 150Pa for both DT and HDT compact and non-compact domains. The remarkable difference between the *E* values calculated in this work and the values reported in the past is due to the fact that a recently proposed model that takes the thickness of the monolayer into account has been used[33]. Thus, by means of force spectroscopy measurements it has been possible to discriminate between the mechanical properties of the alkanethiol monolayers and the properties of the Au(111) substrate.

In summary, in this work we have proven that force spectroscopy in solutions is a powerful tool to study the nanomechanical properties of alkanethiol SAMs on gold, and that this technique turns out to be very sensitive to the molecular packing density.

Acknowledgements

G.O. is recipient of a 'Recerca i Docència' fellowship from the University of Barcelona. This work was supported by grant CTQ2004-08046 from Ministerio de Ciencia y Tecnología (MCYT) and SGR00664 (Generalitat de Catalunya) of Spain. C. V. acknowledges financial support from the Secretaría de Estado de Universidades e Investigación, MEC, Spain.

Reference List

[1] J. C Love, L. A. Estroff, J. K. Kriebel, R. G Nuzzo, and G. M. Whitesides, Chem. Rev. **105**, 1103 (2005).

[2] B. D. Gates, Q. B. Xu, M. Stewart, D. Ryan, C. G. Willson, and G. M. Whitesides, Chem. Rev. **105**, 1171 (2005).

[3] M. Salmeron, Tribol. Lett. **10**, 69 (2001).

[4] R. G. Nuzzo and D. L. Allara, J. Am. Chem. Soc. **105**, 4481 (1983).

[5] L. H. Dubois and R. G. Nuzzo, Annual Review of Physical Chemistry **43**, 437 (1992).

[6] N. Camillone, C. E. D. Chidsey, G. Y. Liu, and G. Scoles, J. Chem. Phys. **98**, 3503 (1993).

[7] P. Fenter, P. Eisenberger, and K. S. Liang, Phys. Rev. Lett. **70**, 2447 (1993)

[8] G. E. Poirier, Chem. Rev. **97**, 1117 (1997).

[9] E. Delamarche, B. Michel, H. A. Biebuyck, and C. Gerber, Advanced Materials **8**, 719 (1996).

[10] C. Vericat, G. Andreasen, M. E. Vela, H. Martin, and R. C. Salvarezza, J. Chem. Phys. **115**, 6672 (2001).

[11] R. G. Nuzzo, E. M. Korenic, and L. H. Dubois, J. Chem. Phys. **93**, 767 (1990).

[12] G. E. Poirier and E. D. Pylant, Science **272**, 1145 (1996).

[13] G. E. Poirier, Langmuir **15**, 3018 (1999).

[14] S. Xu, S. J. N Cruchon-Dupeyrat, J. C. Garno, G. Y. Liu, G. K. Jennings, T. H. Yong, and P. E. Laibinis, J. Chem. Phys. **108**, 5002 (1998).

[15] J. Hautman and M. L. Klein, J. Chem. Phys. **91**, 4994 (1989).

[16] J. Hautman and M. L. Klein, J. Chem. Phys. **93**, 7483 (1990)

[17] T. Hayashi, Y. Morikawa, and H. Nozoye, J. Chem. Phys. **114**, 7615 (2001).

[18] J. Gottschalck and B. Hammer, J. Chem. Phys. **116**, 784 (2002).

[19] X. Torrelles, C. Vericat, M. E. Vela, M. H. Fonticelli, M. A. D. Millone, R. Felici, T. L. Lee, J. Zegenhagen, G. Munoz, J. A. Martin-Gago, and R. C. Salvarezza, J. Phys. Chem. B **110**, 5586 (2006).

[20] S. A. Joyce, R. C. Thomas, J. E. Houston, T. A. Michalske, and R. M. Crooks, Phys Rev. Lett. **68**, 2790 (1992).

[21] K. J. Tupper and D. W. Brenner, Langmuir **10**, 2335 (1994).

[22] J. I. Siepmann and I. R. Mcdonald, Phys. Rev. Lett. **70**, 453 (1993).

[23] E. Barrena, C. Ocal, and M. Salmeron, J. Chem. Phys. **111**, 9797 (1999).

[24] E. Barrena, C. Ocal, and M. Salmeron, J. Chem. Phys. **113**, 2413 (2000).

[25] E. Barrena, C. Ocal, and M. Salmeron, J. Chem. Phys. **114**, 4210 (2001).

[26] J. E. Patterson, A. Lagutchev, W. Huang, and D. D. Dlott, Phys. Rev. Lett. **94**, (2005).

[27] O. Berg and D. Klenerman, J. Am. Chem. Soc. **125**, 5493 (2003).

[28] H. J. Butt, B. Cappella, and M. Kappl, Surface Science Reports **59**, 1 (2005).

[29] C. Vericat, M. E. Vela, J. Gago, and R. C. Salvarezza, Electrochimica Acta **49**, 3643 (2004).

[30] C. Vericat, I. Díez-Pérez, and F. Sanz, (in preparation).

[31] G. Oncins, S. Garcia-Manyes, and F. Sanz, Langmuir **21**, 7373 (2005).

[32] S. Garcia-Manyes, G. Oncins, and F. Sanz, Biophys. J. **89**, 4261 (2005).

[33] E. K. Dimitriadis, F. Horkay, J. Maresca, B. Kachar, and R. S. Chadwick, Biophys. J. **82**, 2798 (2002).

[34] K. Voitchovsky, S. A. Contera, M. Kamihira, A. Watts, and J. F. Ryan, Biophys. J. **90**, 2075 (2006).

[35] E. L. Florin, M. Rief, H. Lehmann, M. Ludwig, C. Dornmair, V. T. Moy, and H. E. Gaub, Biosensors & Bioelectronics **10**, 895 (1995).

[36] G. Nelles, H. Schonherr, M. Jaschke, H. Wolf, M. Schaub, J. Kuther, W. Tremel, E. Bamberg, H. Ringsdorf, and H. J. Butt, Langmuir **14**, 808 (1998).

[37] A. Lio, C. Morant, D. F. Ogletree, and M. Salmeron, J. Phys. Chem. B **101**, 4767 (1997).

[38] X. D. Xiao, J. Hu, D. H. Charych, and M. Salmeron, Langmuir **12**, 235 (1996).

[39] Israelachvili, J. N. *Intermolecular Surface Forces,* 1 ed.; Academic Press: London, 1985.

[40] T. J. Senden and C. J. Drummond, Colloids and Surfaces A: Physicochemical and Engineering Aspects **94**, 29 (1995).

[41] H. J. Butt, M. Jaschke, and W. Ducker, Bioelectrochemistry and Bioenergetics **38**, 191 (1995).

[42] Y. S. Leng and S. Y. Jiang, J. Chem. Phys. **113**, 8800 (2000).

[43] R. Henda, M. Grunze, and A. J. Pertsin, Tribol. Lett. **5**, 191 (1998).

[44] W. J. Price, S. A. Leigh, S. M. Hsu, T. E. Patten, and G. Y. Liu, J. Phys. Chem. A **110**, 1382 (2006).

[45] M. Muraoka and W. Arnold, Jsme International Journal Series A-Solid Mechanics and Material Engineering **44**, 396 (2001).

[46] U. Rabe, M. Kopycinska, S. Hirsekorn, and W. Arnold, Ultrasonics **40**, 49 (2002).

[47] J. Domke and M. Radmacher, Langmuir **14**, 3320 (1998).

[48] H. Hertz and J. Reine, Angewandte Mathematik **92**, 156 (1882).

[49] I. N. Sneddon, International Journal of Engineering Science **3**, 47 (1965).

[50] V. M. Laurent, S. Kasas, A. Yersin, T. E. Schaffer, S. Catsicas, G. Dietler, A. B. Verkhovsky, and J. J. Meister, Biophys. J. **89**, 667 (2005).

[51] E. R. Beach, G. W. Tormoen, and J. Drelich, Journal of Adhesion Science and Technology **16**, 845 (2002).

[52] S. M. Stole and M. D. Porter, Langmuir **6**, 1199 (1990).

[53] M. J. Capitan, J. Alvarez, J. J. Calvente, and R. Andreu, Angewandte Chemie-International Edition **45**, 6166 (2006).

[54] A. B. Tutein, S. J. Stuart, and J. A. Harrison, Langmuir **16**, 291 (2000).

[55] P. T. Mikulski and J. A. Harrison, J. Am. Chem. Soc. **123**, 6873 (2001).

[56] M. Hartig, L. F. Chi, X. D. Liu, and H. Fuchs, Thin Solid Films **329**, 262 (1998).

[57] G. Y. Liuand M. B. Salmeron, Langmuir **10**, 367 (1994).

[58] Q. Du, X. D. Xiao, D. Charych, F. Wolf, P. Frantz, Y. R. Shen, and

M. Salmeron, Phys. Rev. B **51**, 7456 (1995).

Figures

	Initial elastic region (Hertz-Sneddon model)	Initial elastic region (Dimitriadis model)	Final elastic region (Hertz-Sneddon model)	Final elastic region (Dimitriadis model)
Decanethiol	3±2MPa	61±14Pa	16±5MPa	81±44Pa
Decanethiol compact	17±4MPa	44±22Pa	62±10MPa	55±15Pa
Hexadecanethiol	5±10MPa	64±23Pa	20±6MPa	50±68Pa

Table 1. E values for the initial and final elastic regions depicted in Fig.4 using Hertz-Sneddon and Dimitriadis models.

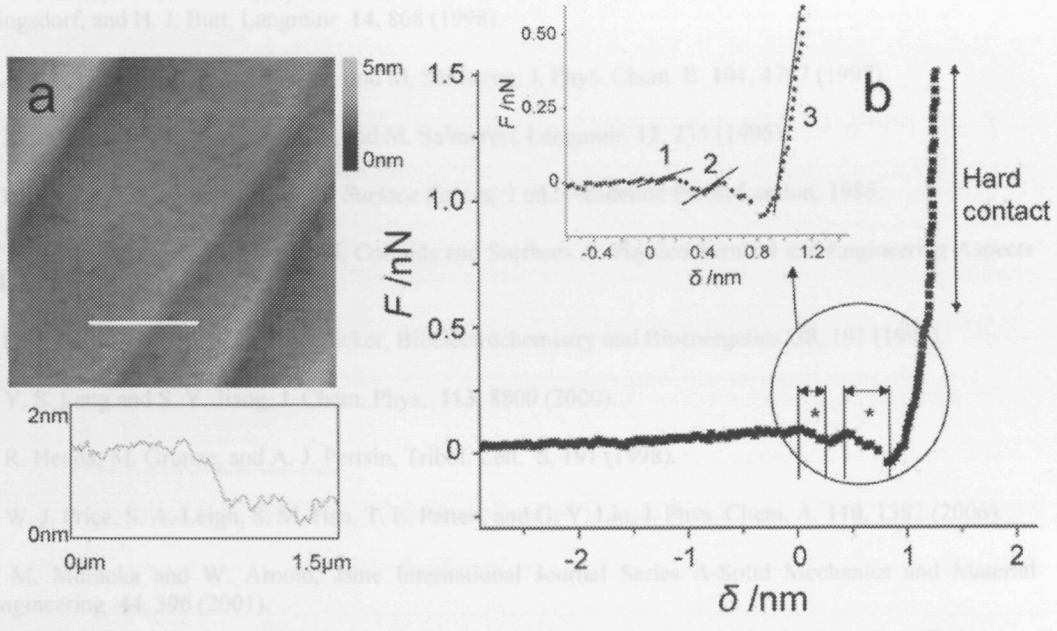

Fig.1. a) 5x5μm2 AFM topographic image of a decanethiol (DT) monolayer deposited on an Au(111) surface in 0.1M KOH electrolyte solution. Height section (white line in the image) shows the presence of defects on the monolayer (non-compact) and Au steps. b) Fvδ curve for the same DT monolayer on Au(111) in KOH solution. Sudden penetration events are marked with a *. Inset: zoom of the contact region. 1 and 2 correspond to elastic compression regions prior to a sudden penetration event. Region 3 corresponds to the maximum compression of the tip prior to "hard" contact with the sample.

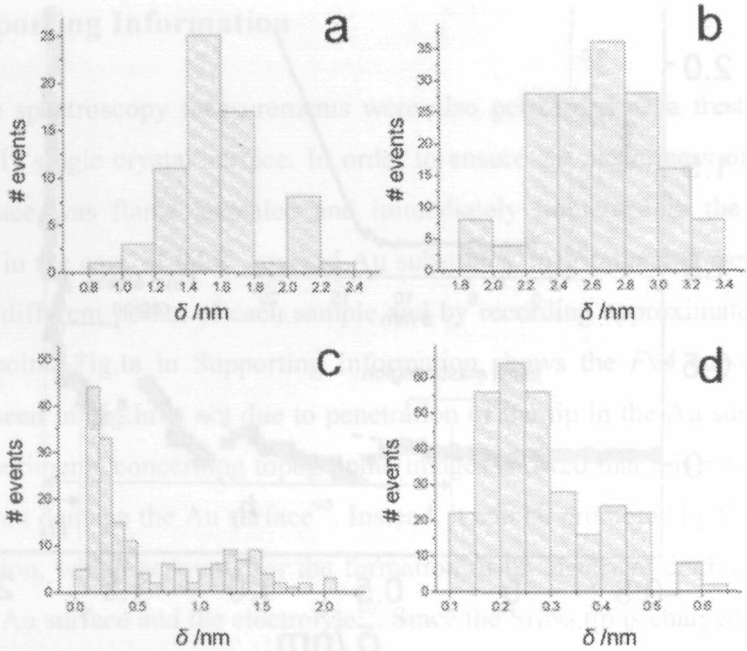

Fig.2. Histograms that represent the total penetration values measured in *Fvδ* curves obtained on a) DT and b) HDT monolayers. c) and d) are the histograms that represent the penetration during all sudden penetration events (marked with a * in Fig.1b) detected in *Fvδ* curves obtained on DT and HDT, respectively.

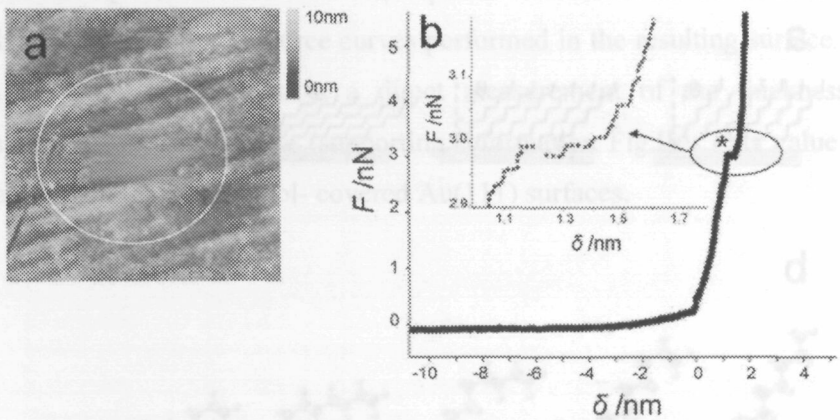

Fig.3. a) 10x10μm2 image of a compact domain in a DT monolayer on an Au(111) surface in 0.1M KOH solution. b) Fvδ curve obtained on the compact DT domain. The breakthrough of the monolayer is marked with a *. Inset: zoom of the breakthrough region, where individual sudden penetration events can be detected.

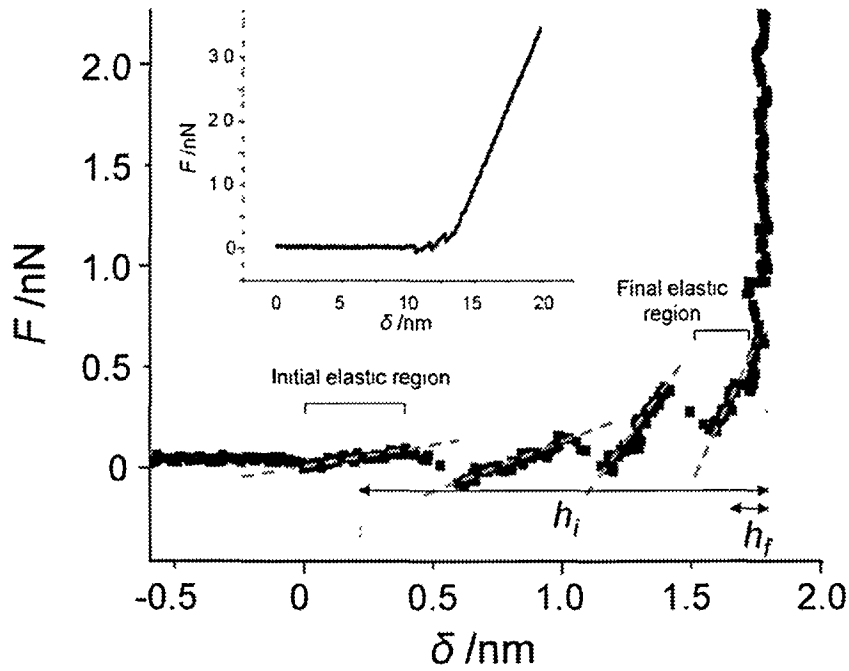

Fig.4. Fvδ curve obtained on a non- compact region of a DT monolayer on Au(111) in 0.1M KOH solution. hi and hf are the monolayer thicknesses used to calculate E by means of Dimitriadis model in the initial and final elastic regions respectively. Inset: raw vertical force vs. piezo displacement curve.

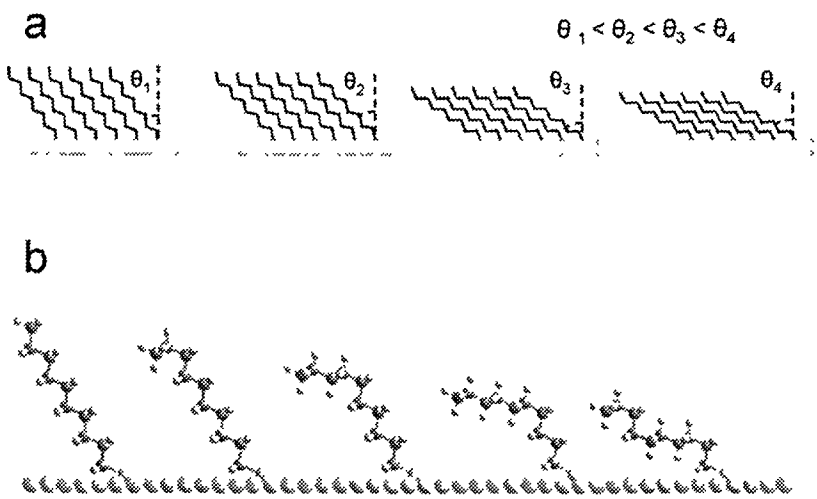

Fig.5. a) Alkanethiol monolayer folding mechanism that maximizes Van der Waals interaction between hydrocarbon chains, resulting in quantized folding angles. b) Gauche defects in the DT monolayer due to compression. Only the most energetically favorable gauche defects have been depicted.

Supporting Information

Force spectroscopy measurements were also performed on a freshly prepared, clean Au(111) single crystal surface. In order to ensure the cleanliness of the sample, the Au surface was flame annealed and immediately immersed in the 0.1M KOH solution. As in the case of thiol- covered Au substrates, measurements were performed in at least 5 different points of each sample and by recording approximately 100 force curves per point. Fig.Ia in Supporting Information shows the $Fv\delta$ curve. The small penetration seen in Fig.Ia is not due to penetration of the tip in the Au surface because previous experiments concerning topographic images showed that this range of vertical forces does not damage the Au surface[90]. Instead, it can be promoted by the presence of ions in solution, which accounts for the formation of an electrical double layer (EDL) between the Au surface and the electrolyte[40]. Since the Si_3N_4 tip is charged[41,91] at the pH of the experiment, there is some repulsion as the tip crosses the EDL. This repulsion is translated into a tip deflection that is seen as a small penetration in $Fv\delta$ curves.

To test the influence of contamination in the $Fv\delta$ curves, the Au surface was rinsed with MilliQ water, dried with Ar, exposed to ambient for 10 minutes and then covered by the KOH solution. Force curves performed in the resulting surface rendered δ values of 4.2±1.2nm, which is a direct measurement of the thickness of the contaminant layer on the surface (supporting information Fig.Ib). This value is much larger than that found for the thiol- covered Au(111) surfaces.

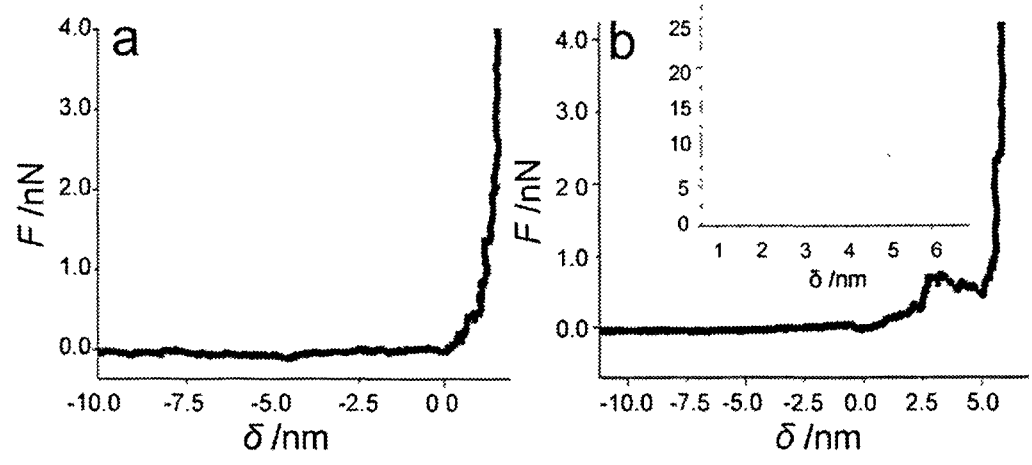

Fig.I. a) Fvδ curve obtained on an Au(111) single crystal surface immersed in 0.1 M KOH electrolyte solution. b) Fvδ curve obtained in 0.1 M KOH solution on the same surface after 5 min exposure to air. Inset: Histogram that represents the total penetration values (in nm) measured in Fvδ curves obtained in 0.1M KOH on an Au(111) surface previously exposed to air for 5min. δ values were calculated as the total penetration from the contact between sample and surface to the "hard" contact between the tip and the Au(111) surface and represents the thickness of the soft material (contamination) deposited on the substrate.

Tilting model				
Tilt angle (θ)	Height (Å)		Thickness diminution (ΔÅ)	
	decanethiol	hexadecanethiol	decanethiol	hexadecanethiol
35	12 2	18 4	-	-
43	10.9	16.5	1.3	1.9
55	8 6	13.0	2.3	3.5
59	7.7	11.5	0.9	1.5

Table I. DT and HDT monolayer thicknesses as function of the molecular tilting angle. The angles were calculated in order to maximize the hydrocarbon chain interlocking (2D model). Height diminution represents the height decrease between a folding event and the next one.

Gauche defects				
	Height (Å)		Thickness diminution (ΔÅ)	
	decanethiol	hexadecanethiol	decanethiol	hexadecanethiol
Trans	15.0	22.6	-	-
G+	13.6	21.2	1.4	1.4
G+g+	11.0	18.6	2.6	2.6
G+g+g+	9.0	16.6	2.0	2.0
G+g+g+g+	7.0	14.6	2.0	2.0

Table II. DT and HDT monolayer thicknesses as gauche defects are introduced in the hydrocarbon chain. Height diminution represents the height increment between the creation of a gauche defect and the next one.

4.6.4 Nanomechanical properties of arachidic acid Langmuir-Blodgett films

G. Oncins[a], J. Torrent-Burgués[b], F. Sanz[a]

[a]Department of Physical Chemistry, Universitat de Barcelona and Center of Nanobioengineering of Catalonia (CREBEC), Martí i Franquès 1, 08028 Barcelona, Spain

[b]Department of Chemical Engineering, Universitat Politècnica de Catalunya, Colom 1, 08222, Terrassa (Barcelona), Spain

Submitted to Journal of Physical Chemistry B

4.6.4.1 Summary

This is perhaps one of the most fundamental works presented in this thesis, as it explores the intermolecular interactions that arise in a model monolayer as it can be a fatty acid Langmuir-Blodgett films.

To begin with, we studied the topography of Langmuir-Blodgett films of arachidic acid extracted at different surface pressures corresponding with a) the acid in the gas - LC phase, b) the acid in the LC phase and c) the acid in the S phase. Force Spectroscopy and friction experiments were performed on samples extracted at the cited surface pressures in order to assess if the observed topographical changes had any nanomechanical correspondence. The obtained results can be summarized as follows:

- *The arachidic acid monolayer thickness depends on the extraction surface pressure (the thickness increases as the surface pressure increases) and the thickness change takes place in discrete steps. Considering the molecular tilting model proposed by Barrena et al.[218], the obtained monolayer thicknesses*

coincide nicely with the predicted tilting angles, so we concluded that the van der Waals interactions forces between chains play and important role in the final monolayer structure.

- *The monolayers break under the exertion of a vertical compression (Δx vs. Δz curve) and the measured F_y value increases as the monolayer thickness increases. Energetic estimations inferred from the experimental measurements suggest that the increment in van der Waals interactions due to the high compactness of monolayers extracted at high surface pressures is not enough to explain the F_y value increment, so we propose that the electrostatic interactions between the carboxy- and carboxylic acid groups are crucial for the mechanical resistance of the monolayer.*

- *F_f vs. F_v curves performed on arachidic acid monolayers reveal three nanotribological regimes; at low F_v values, the tip scans the outer sample surface without changing the monolayer structure. Because of the hydrophilic nature of the tip and the hydrocarbon chains hydrophobicity, the interaction between them is weak and the F_f value is extremely low. Then, as a certain threshold F_v is reached, F_f signal increases noticeably, as well as the μ value. Topographic AFM data suggests that during this regime the monolayer is plastically deformed by the tip. The last regime corresponds to the contact between the tip and the substrate.*

Nanomechanical properties of arachidic acid Langmuir-Blodgett films

Gerard Oncins[1], Joan Torrent-Burgués[2], Fausto Sanz[1]*

[1]*Department of Physical Chemistry, Universitat de Barcelona and Center of Nanobioengineering of Catalonia (CREBEC), Martí i Franquès 1, 08028 Barcelona, Spain*

[2]Department of Chemical Engineering, Universitat Politècnica de Catalunya. Colom 1, 08222, Terrassa (Barcelona), Spain

goncins@ub.edu

ABSTRACT

The nanomechanical properties of Langmuir-Blodgett films of arachidic acid extracted at surface pressures of 1, 15 and 35 mN/m and deposited on mica are investigated by Atomic Force Microscopy, Force Spectroscopy and Lateral Force Microscopy. It is experimentally demonstrated that the molecular ordering of the arachidic acid depends on the extraction pressure. According to this, tilting angles of 50°, 34° and 22° are detected and identified as conformations that maximize van der Waals interactions between the arachidic acid alkyl chains. The vertical force needed to puncture the monolayer strongly depends on the molecular tilting angle, ranging from 13.07±3.24 nN at 1 mN/m to 22.94±5.49 nN at 35 mN/m. The different interactions involved in the monolayer cohesion are discussed and quantitatively related with the experimental monolayer breakthrough forces. The friction measurements performed until monolayer disruption reveal three friction regimes corresponding with a low friction elastic monolayer deformation at low vertical forces followed by a sharp increase in friction force due to a sudden plastic deformation of the monolayer. The last regime corresponds with the monolayer rupture and the contact between tip and substrate. The friction coefficient of the substrate is seen to depend on the extraction pressure, fact that is discussed in terms of the relationship between the sample compactness and its rupture mechanism.

KEYWORDS

Monolayers, fatty acids, nanotribology, friction, force spectroscopy, force curves.

INTRODUCTION

Since its development in 1935[1], the Langmuir-Blodgett technique (LB) has been widely used to prepare all kind of ordered structures as varied as phospholipid bilayers[2] or nanowire arrays[3]. The possibility to control the surface pressure and consequently the area per molecule during the transference to a solid substrate makes of this technique a powerful way to prepare surfaces with tailored chemical, structural and mechanical properties. This fact, besides the awakening of Micro- and NanoElectromechanical systems (MEMS and NEMS) and the consequent necessity to produce lubricants at a molecular level have led to an extensive use of LB films, not only to obtain viable low-friction coatings for the electronics industry[4,5] but also to use them as models to study molecular interactions and interfacial phenomena. For these applications, fatty acid LB films have become useful systems because of their linear geometry, amphiphilic nature and high mechanical stability and durability.

Down to the micro- and nanometric range, fatty acid mono- and bilayers have been studied by Atomic Force Microscopy (AFM) and related techniques such as Lateral Force Microscopy (LFM), which was applied in the past to a variety of films on surfaces[6-11] such as lipid bilayers and membranes[12;13], specially stressing the chemical, compositional and structural differentiation LFM is sensitive to.

Concerning the molecular structure of fatty acid LB films, the cadmium arachidate (CdAr) pattern was resolved using diffraction techniques[14], showing a hexagonal compact packing with the alkyl chains perpendicular to the surface. Posterior IR studies concluded that the chains were in an all-trans conformation[15]. Related AFM molecular resolution studies conducted by Mori et al.[16] confirmed the perpendicularity and hexagonal packing structure of arachidic acid (AA) LB films extracted at 25 mN/m. Interestingly, Evenson et al.[17] concluded that the alkyl chain tilt angle depended on the extraction pressure, as well as on the area per molecule. In this direction, Kajiyama et al.[18] experimentally demonstrated the concordance between the calculated area per molecule before and after transferring lignoceric (LA) and stearic acid (SA) monolayers to the substrate. X-ray studies performed on behenic acid (BA) LB films suggested that the film structure was irrespective of the phase from which deposition took place[19] and Chunbo et al.[20] reported that 1,2-Dipalmitoyl-sn-Glycero-3-Phosphate mono- and trilayers relax to match the mica atomic structure, but a more recent work concluded that the nanomechanical properties of AA, BA and SA strongly depend on the extraction pressure[21].

The dependence between monolayer thickness and applied vertical force (F_v) was studied for several fatty acids, showing that there is an initial thickness decrease attributed to the creation of gauche defects in the alkyl chains terminal ends at low F_v, followed by a constant thickness regime and by a final monolayer rupture after a threshold F_v is reached[21]. A similar study performed on BA[22] pointed out that the monolayer thickness evolution vs. F_v also depended on the monolayer phase, which can be controlled both by changing temperature or extraction pressure. Different monolayer phases respond with different friction force (F_f) vs. F_v trends, showing that F_f is highly sensitive to the monolayer molecular ordering and concluding that solid BA monolayers behave elastically at low F_v and deform plastically as F_v increases, while liquid BA shows plasticity independently of the applied F_v[23].

Although the presence of defects plays a crucial role in the tribological performance of fatty acid monolayers[24], the composition of the subphase in the Langmuir film (prior to deposition on a solid substrate) is also important: carboxylic acid groups create H-bonding networks at acid pH[16], contributing to a better molecular packing. For higher pH values, the stability of the monolayer can also be increased adding cations, which bind electrostatically to the deprotonated carboxyl groups, as it was experimentally proved studying the sample relaxation time after collapse[25]. Another important factor concerning the mechanical properties of LB monolayers is the length of the alkyl chain, which modifies the intermolecular van der Waals interactions. Then, the longer the chain, the higher the F_v at which the monolayer breaks during scanning[21]. Van der Waals interactions can also be modified varying the extraction pressure, factor that also modifies the monolayer frictional behavior[26].

The chemistry of the interface tip-monolayer also modifies the friction response, which is much higher for tip-carboxylic acid than for tip-alkyl chain (this effect was seen in a multilayered SA sample, detecting friction differences between even and odd layers[27]). At the same time, tip-alkyl chain friction response is much lower than tip-SiO_2, fact that was used in a pioneer work to distinguish CdAr covered areas and the SiO_2 substrate[24].

The aim of the present work is three-fold: firstly, we focus on the topography of AA monolayers extracted at different surface pressures in order to examine the relationship between the surface-pressure vs. area isotherm and the molecular conformation after the monolayers are supported on mica to obtain information about the molecular tilting angle and their morphology. Secondly, the nanomechanical properties of these monolayers under vertical compression are tested performing force spectroscopy to measure the mechanical resistance of the monolayers vs. extraction pressure and to assess the different role of van der Waals and electrostatic interactions in the monolayer cohesion. And thirdly, the nanotribology is studied by means of F_f vs. F_v curves to gain insight about the different frictional stages that range from non-contact to the total disruption of the monolayer.

EXPERIMENTAL METHODS

Langmuir-Blodgett film preparation

Langmuir films were obtained in a NIMA 1232D1D2 Langmuir-Blodgett trough (area = 1200 cm^2). Pure water (Millipore MilliQ grade) was used as subphase. A solution of AA 3.2 mM in chloroform was spread over the water subphase and 15 min were lag before compression in order to permit evaporation of the chloroform. The compression speed was set to 50 cm^2/min (2.5 cm/min, 5.2 $Å^2$/molec/min). The LB films were transferred at constant pressure onto freshly cleaved atomically flat mica surfaces (1 cm x 1 cm sheets). The transfer was done using a NIMA 1232 D1 dipper at several surface pressures and at a constant temperature of 24°C. LB films were obtained following a Z deposition and at an extraction speed of 10 mm/min. The measured transfer ratios were close to 100%.

AFM topographic measurements

Topographic images, force spectroscopy and friction measurements were performed in contact mode with a Dimension 3100 microscope attached to a Nanoscope IV controller (Digital Instruments, Santa Barbara, CA). For topographic measurements, Si_3N_4 triangular tips (OMCL TR400PSA, Olympus, Japan) with a nominal spring constant of 0.02 N/m were used. Force curves were performed before and after scanning the sample to ensure that captured images were acquired at minimum F_v. The whole system was enclosed in a metallic isolation box placed on a vibration isolation table (TMC, Peabody, MA). During all experiments, temperature and humidity were controlled and maintained at 20-22°C and 40-50%RH.

Force spectroscopy

Triangular Si_3N_4 tips with a nominal spring constant of 0.5 N/m were used (Microlever Probes model MLCT-AUNM, Veeco, Camarillo, CA). Vertical force constant (k_v) was calculated for each tip individually using the thermal noise method[28] in a Force Probe1-D MFP microscope (Asylum Research, Santa Barbara, CA). Force curves were performed using the Force Volume routine implemented in the Nanoscope software, which performs a grid of single force curves in a selected area, ensuring that each force curve is done in a fresh spot. The data analysis was performed with the AFM Force Volume Data Analysis Software[29]. The penetration depth (or sample penetration) during a force curve was calculated as

$$penetration\ depth = \Delta Z - \Delta x \tag{1}$$

being ΔZ the piezo displacement and Δx, the cantilever deflection in the contact region. Then,

$$\Delta x = \Delta V / S \tag{2}$$

where ΔV is the increment in photodetector vertical signal as the tip contacts the sample and S is the sensitivity, which is the slope of the contact region of a force curve performed on a rigid sample.

LFM measurements

The individual lateral constant (k_l) of each probe was calculated using the Ogletree et al. method[30]. Briefly, a silicon oxide grid with very sharp ridges (Mikro-Masch TGG01) and known geometry is scanned by the tip while the lateral deflection in the trace and retrace scans is recorded. As the two sides of the ridge are made from the same material, the friction difference between the trace and retrace scans is directly related to the ridge slopes and cantilever k_l.

Friction force vs. vertical force curves (F_f vs. F_ν) were performed as follows: an ascending saw tooth signal from an external function generator (Agilent, Palo Alto. CA) was subtracted from the vertical photodetector signal obtained through the Signal Access Module (Digital Instruments, Santa Barbara, CA) using a home-made electronic card. Then, the resulting voltage was injected to the vertical photodetector signal through the Signal Access Module, allowing the feedback loop on the vertical deflection to maintain a steadily increasing F_ν over the course of a F_f vs. F_ν experiment. The cantilever scan area was set to 300 x 300 nm^2 at 6.1 Hz with a 512 x 512 pixel resolution. As a result, a whole F_f vs. F_ν curve ranging from low to high F_ν values was obtained every 84 seconds. Further experimental details can be found elsewhere[31]. The whole data treatment was performed using the Matlab scripts provided by Carpick's group[32].

RESULTS AND DISCUSSION

Monolayer morphology and alkyl chain orientation vs. extraction pressure

Fig. 1 shows the AA monolayer isotherm and the contact AFM images corresponding to monolayers extracted at pressures of a) 1 mN/m, b) 15 mN/m and c) 35 mN/m. It is clear that the morphology of the monolayers depends on the extraction pressure: at 1 mN/m, the AA molecules arrange in a homogeneous monolayer with voids, indicating that the surface is not totally covered. At 15 and 35mN/m the monolayer completely covers the mica surface and the presence of higher domains is detected, with an increasing domain area ratio as the extraction pressure increases. The heights of the monolayer and the observed domains were measured at each extraction pressure and plotted in Fig. 2a. The height measurements were performed using the bearing option of the Nanoscope software on an area that contained a hole and a piece of monolayer. This option plots the height of each pixel respect to the lowest one, obtaining a height histogram of the selected area. In the samples where the substrate was fully covered, that is, 15 and 35 mN/m, a 1 x 1 μm^2 area was scratched to expose the mica surface. The grey dots in Fig. 2a correspond to the analysis of individual images captured on different regions of the

sample and over 3 different samples to ensure reproducibility. Interestingly, the monolayer heights correspond with discrete values in the 3 referred extraction pressures: at 1mN/m, the unique monolayer height is 17.5±0.4 Å; at 15 mN/m, 17.4±0.4 Å and 22.4±0.2 Å (24.8±0.2 Å domains were sporadically observed) and at 35 mN/m, 22.4±0.2 Å and 25.0±0.1 Å. Height values lead to two conclusions: first, the domains height tends to be higher as pressure increases and second, monolayers extracted at different pressure share structures with common height values. The first conclusion can be correlated with the isotherm shown in Fig. 1. At 1 mN/m, AA molecules are in the low surface pressure region of the liquid condensed phase and AFM images reveal that molecules aggregate and coalesce forming a continuous monolayer with an average area per molecule of 25 $Å^2$. Considering that the molecules arrange in a hexagonal lattice[14], the calculated distance between hydrocarbon chains at 1 mN/m is 5.5 Å, which exceeds the 4.0 Å[33] that corresponds with the minimum distance between $-CH_2$ groups in adjacent molecules[34]. This higher value of area per molecule leads to a molecular tilting that was studied in the past by means of NEXAFS[35,36], RAMAN[37,38] and FTIR-ATR[39] for a wide variety of fatty acids. Nevertheless, there is a certain discrepancy between the reported tilting angles, mostly attributed to variations in temperature, substrate or extraction conditions used by the different authors. As pressure increases (15 mN/m), the monolayer, formally in the liquid condensed phase of the isotherm, forms domains of a new and more compressed liquid condensed phase with an area per molecule of 22 $Å^2$ and an intermolecular distance of 5.0 Å. Finally, at a pressure of 35 mN/m and the AA monolayer formally in the solid phase, the area per molecule reduces to 19 $Å^2$ and the intermolecular distance to 4.7 Å. Besides, a still lower tilting angle appears. In order to quantify the observed molecular tilting angles we considered an AA maximum molecular height of 27.0±0.1 Å, which was experimentally measured in our samples near mica defects, which presumably acted as nucleation points where surface pressure built up. This experimental AA total length is in excellent agreement with the reported values[16,40]. Now, relating the experimental monolayer heights with the total length of the AA molecule, tilting angles of 50° at 1 mN/m, 51° and 34° at 15 mN/m and 34° and 22° at 35 mN/m are obtained. The significance of molecular tilting discretization was explored by a pioneering work from Outka et al.[41], who suggested that cadmium and calcium arachidate film height was determined by the interlocking of hydrocarbon chains at certain angles which maximize van der Waals interactions, proposing a simple geometrical model to predict the possible orientations. This model was verified for alkylsilanes on mica, were molecules tilted in a discrete way as pressure was applied by an AFM tip. Alkanethiols on gold were also observed to fold[42] and the authors proposed a similar model, which was lately improved to account for tilting angles in 2 dimensions[43,44]. This 2D model is applied in the present paper to explain the experimental AA tilting angles. To do that, it is considered that the intermolecular distance at any tilting angle is constant and equal to the minimum distance between two alkyl chains (4.0 Å). This assumption is more plausible in LB films and alkanesilanes because they are not chemically attached to the

substrate, so individual molecules can rearrange and modify their molecular area to some extent to maximize the interaction between the alkyl chains. In the case of alkanethiols on gold, and in order to maintain a constant distance between alkyl chains, the distance between the thiol groups must change, which is not evident because of the covalent bond between the thiols and the gold.

The tilting angles predicted by the 2D model are depicted in Fig. 2a as horizontal straight dotted lines[45]. The excellent fitting between the experimental data and the predicted tilting angles suggest that alkyl chains are highly oriented and that this orientation is strongly controlled by van der Waals interactions as schematically drawn in Fig. 2b. It is noticeable to find a coexistence of different molecular tilting angles in the same sample, fact that can be explained by the presence of substrate defects that induce local surface pressure increments. We also observed that sample ageing[46] influences the morphology of the samples: the area ratio corresponding with 34° and 22° domains increased with time both in the 15 mN/m and 35 mN/m samples. Consequently, the presence of lower tilting angles (thicker monolayer) is favored with time, meaning that the monolayer keeps on rearranging after being deposited. The quantification of the rearrangement process and the factors that influence it will be studied in a forthcoming work.

Force Spectroscopy Measurements

Force Spectroscopy has proved to be a very useful technique to test the mechanical properties of a variety of thin films[47] and biological structures[48,49]. The experimental procedure consists on the application of a vertical compression on the sample by an AFM probe while the cantilever deflection is recorded both in the approach and retract processes, so sample compression and relaxation can be sensed and monitorized. One of the figures of merit of force curves is the breakthrough force (F_y), which is the necessary F_y to break the sample structure[50]. Sample breakthrough was reported in several papers, mostly concerning soft biological structures as phospholipid bilayers[51]. Interestingly, F_y can be regarded as a sample fingerprint because it is highly sensitive to structural changes induced by temperature variations, phase transitions[52] or ionic strength changes in the medium[53]. For all this, it is clear that breakthrough events detection and F_y quantification can render important information about the different forces that interplay in the structural layout of fatty acid structures.

So as to test the mechanical properties of the AA monolayer and to assess the dependence of F_y with the extraction pressure and, hence, with the tilting angle, force curves were performed on samples extracted at 1, 15 and 35 mN/m. In the samples extracted at 15 mN/m, the force curves were performed on the 34° tilted phase while in the 35 mN/m sample, due to the high degree of phase mixing (Fig. 1c), force curves were performed both on the 34° and 22° tilted phases. To give an example, a F_y vs. penetration depth curve performed on a 35 mN/m AA monolayer is shown in Fig. 3; initially, the tip and sample are not in contact (white dots). We must emphasize that in this region equation (1) can not be

applied, so the negative penetration must be understood as the probe approaching the monolayer. Then, as the tip contacts the sample (grey region), the tip deflects as more F_y is applied until an abrupt penetration event (sample breakthrough F_y) takes place around 20 nN. Finally, the tip contacts the mica substrate after rupturing the sample (black dots region). The total sample penetration, considered as the sum of penetration depth both in the grey region and in the breakthrough event, equals the monolayer thickness. Force curves performed on the different domains observed in samples extracted at 15 mN/m (50° and 34° domains), are distinguished due to the difference in the value of the monolayer thickness, but it is not possible to discriminate between the force curves performed on each of the two phases observed in the 35 mN/m sample (34° and 22° domains) by means of the penetration depth values because dispersion of these values is wider than the height difference between the two phases.

Fig. 4 shows the F_y values for AA monolayers at different extraction pressures. Each histogram contains measurements performed with two individually calibrated tips on 5 different surface spots each, giving F_y values of 13.07±3.24 nN, 15.34±4.94 nN and 22.94±5.49 nN for 1, 15, and 35 mN/m samples respectively. Then, it is clear that the monolayer resistance to be punctured increases with the monolayer thickness, that is to say, as the molecular tilting decreases. Interestingly, F_y is also highly dependent on the monolayer phase; while 1 and 15 mN/m samples are in the liquid condensed phase (F_y values are very similar for the two extraction pressures), the sample extracted at 35 mN/m is in the solid phase (significantly higher F_y value). Due to the F_y sensitivity to structural changes, the energetic interactions between the AA molecules depending on the different molecular packing of each phase can be correlated with the force spectroscopy results. As it was proposed by Israelachvili et al.[34], the total van der Waals interaction between neighbor alkyl chains equals the energy between adjacent $-CH_2$ groups, which is 6.9 kJ/mol for an intermolecular distance of 4.0 Å, multiplied by the number of $-CH_2$ groups per molecule that interact favorably. This model leads to a maximum interaction when the tilting angle is 0°, while the number of favorable $-CH_2$ interactions is reduced by one as the alkyl chains slip one notch to accommodate to the next possible tilting angle[42]. According to this, calculated van der Waals energies at 22°, 34° and 50° are 127.7, 124.2 and 117.3 kJ/mol respectively[54], which represents that at 34° and 50° the van der Waals interaction is 97% and 92% of the interaction at 22°. The experimental total energy exerted by the tip on the monolayer (E_e) to rupture it can be calculated as

$$E_e = F_y * penetration\ depth \tag{3}$$

If E_e values are normalized the same way, the force to break the monolayer at 34° and 50° is 64% and 47% of the E_e at 22°[55]. Consequently, it is clear that the F_y increment as tilting angle reduces can not be explained only as a function of the van der Waals interactions between the chains and that other cohesive forces that also depend on extraction pressure have to be considered. Indeed, the role of the

hydrophilic headgroups in the stability of the monolayers was studied in the past. The presence of hydrogen bonds was detected both between amide[56] and carboxylic acid groups in multilayers, increasing the transition temperature[57]. The interaction between the polar headgroups and the substrate surface is also important and influences the thermal stability of the monolayers[58;59]. Moreover, as the AA pKa is 7.1 and the subphase used in the present experiments is milliQ water, the acid groups will be partially deprotonated, interacting electrostatically with both the charged mica surface[60] and the other carboxylic groups. The energetic study of protonated and deprotonated fatty acid monolayers performed by Tippmann et al.[61] reported thermal desorption energies of 185 and 76 kJ/mol for magnesium arachidate and AA respectively, highlighting the significance of electrostatic charges in the structure of the monolayers. Moreover, the monolayer tilting angle was observed to change when switching from SA monolayers to cadmium stearate due to electrostatic interactions[62], fact that was also observed by Outka et al[41] with cadmium and calcium arachidate monolayers. In conclusion, the electrostatic interaction arisen between the partially deprotonated carboxyl groups, between these groups and the charged mica surface and the hydrogen bonds between carboxylic acids strongly contribute to the mechanical resistance of AA monolayers.

The dispersion of F_y values for a certain extraction pressure is an important parameter because it is directly related with the fluidity and homogeneity of the monolayer. Previous studies performed in our group concerning the mechanical properties of a variety of phosphatidylcholine bilayers, demonstrated that the F_y dispersion was always lower when the phospholipid was in liquid phase than when it was solid[52]. As the sample remains fluid, the surface is more homogeneous because of the high mobility of the molecules. Then, the mechanical properties of the sample are irrespective of the spot where the force curve is performed, which results in a low F_y dispersion. As the sample is cooled down and becomes solid, defects and inhomogeneities arise in the structure, contributing to a larger dispersion of mechanical properties from spot to spot. In relation to the results presented in this paper, the dispersion of the 1 mN/m histogram is the lowest of the three, as this is the sample with weaker intermolecular interactions and higher area per molecule. This fact leads to an increased fluidity respect to the other samples, especially the one extracted at 15 mN/m. At 35 mN/m, the dispersion is promoted by the tight molecular packing but also because of the presence of two mixed phases.

In conclusion, force spectroscopy measurements have proved to be suitable to assess the mechanical stability of AA monolayers and to relate it with their molecular orientation. Moreover, and to the best of our knowledge, this is the first study that experimentally quantifies the difference in mechanical properties between monolayers that only differ in their molecular tilting angle. A further work will be devoted to study and isolate the contribution of van der Waals forces, hydrogen bonds and electrostatic interactions to the F_y results so as to quantify them separately and relate them to the structural resistance of the monolayer.

F_f vs. F_v measurements

Fig. 5 shows three representative F_f vs. F_v curves performed on AA samples extracted at 1, 15 and 35 mN/m (in the 15 and 35 mN/m samples. F_f vs. F_v curves were done on the 34° and 22° tilted phases respectively). All F_f vs. F_v curves were performed from $F_v = 0$ nN up to total monolayer disruption, as it can be seen in the topographic images shown in Fig. 5.1 and Fig. 5.2. Regardless of the extraction pressure, all curves show the same general shape. At low F_v, there is a linear region with low F_f, which ends with an abrupt F_f increase followed by another linear region with a higher slope than the one observed at low F_v. Finally, the slope reduces again and another linear region appears. These regimes correspond with different tribological processes induced by the increasing F_v and are schematically depicted in the Fig. 5 inset. The first regime corresponds to the contact between the tip and the top of the monolayer (Fig. 5 inset a). As the Si_3N_4 tip is hydrophilic and the AA chains are hydrophobic, F_f is extremely low. Besides, part of the low F_f recorded for all extraction pressures at F_v~0 nN, ca. 2 nN, can be attributed to adhesive forces promoted by water on the tip apex, as the experiments were performed in air. Very low F_f at low F_v was also observed in behenic acid and stearic acid monolayers and attributed to an elastic deformation regime[27]. These results were supported by molecular dynamics simulations, which predicted that alkyl chains could be compressed up to 25% of its total length without deforming plastically[63].

As F_v increases, the monolayer cannot withstand its initial structure and deforms plastically (Fig. 5 inset b). This effect was seen in the past in alkanesilane monolayers[64] and alkanethiols on gold[44], where the molecules tilted in a quantized way as a response to the increasing pressure. According to this, we propose the model depicted in Fig. 6 for the behavior of AA monolayers under compression. As a certain F_v is reached, the tip can deform the molecules plastically as it scans the sample surface (Fig. 6b) and slides not *on* the monolayer but *in* the monolayer, tilting the molecules as it moves. This interaction greatly increases the area of contact between the tip and the surrounding molecules, fact that, besides the resistance offered by the molecules that are in front of the tip in the initial tilting conformation, leads to a F_f increment. The topography of the monolayer after performing a F_f vs. F_v curve (Fig. 6) reveals the plastic deformation induced in the monolayer. Interestingly, the molecules do not recover the initial conformation after the F_v is released (Fig. 6b section), so possibly they tilt in a quantized way to maximize the chains interlocking. Unfortunately, as the k_v of the tips used for friction measurements is too high, no reliable height measurements could be done in order to calculate the tilting of the molecules in this friction regime. Once the tip has entered the monolayer, F_f increases linearly until a certain F_v is reached and the monolayer is thoroughly punctured and removed from the surface so the tip contacts the substrate, which also results in a linear relationship between F_f and F_v.

In order to extract quantitative information from the F_f and F_v curves, experiments were performed in two different samples with two vertically and laterally calibrated cantilevers. At least 20 F_f and F_v curves were recorded for each tip, sample and extraction pressure. The chosen figures of merit to quantify the curves were the increment of vertical force during friction on top of the monolayer, which corresponds with Fig. 5 inset a) region (ΔF_{vTM}), its slope (μ_{TM}) and the slope of the F_f and F_v curves when the monolayer is broken and the tip contacts the substrate, Fig. 5 inset c), (μ_S). These measurements are shown in Fig. 7, where grey dots correspond to individual measurements and white dots are the mean values. Concerning ΔF_{vTM} (Fig. 7a), it is clear that its value increases with extraction pressure. This means that the F_v needed to rupture the monolayer increases as the area per molecule and the tilting angle decreases. As a consequence, F_f vs. F_v curves are sensitive to the molecular packing and are able to discern between the different arrangements that AA molecules undergo depending on the extraction pressure. In fact, these measurements corroborate the force spectroscopy data presented in Fig. 4, where F_v is a measurement of the mechanical strength of the monolayer. Nevertheless, it has to be considered the different nature of the two mechanical tests; force spectroscopy applies a F_v in a spot, affecting a small number of molecules. Friction measurements affect a larger number of molecules and, although an increasing F_v is also applied, at the same time the tip moves laterally. Then, it is clear that the relationship between F_v and ΔF_{vTM} is not straightforward and is affected by a number of factors as tip velocity and scan area. However, it is interesting to note that force spectroscopy and friction measurements give complementary information about the mechanical resistance of monolayers and are sensitive to different packing densities.

The relationship between F_f and F_v is linear for region a) and c) in Fig. 5 inset, so μ_{TM} and μ_S can be regarded as the friction coefficients of the monolayer and substrate respectively. Concerning μ_{TM}, Fig. 7b shows that it decreases as extraction pressure increases, ranging from 0.35 to 0.18. The decrease can be explained according to the different compactness of the tested monolayers. At low extraction pressures the number of structural defects and vacancies is high in the monolayers as shown in Fig. 1a, where micrometric holes are seen in the sample. As is well known, packing defects are prone to increase F_f, as the structure provides more pathways to dissipate energy during sliding[65]. As extraction pressure increases, molecules pack more tightly and both μ_{TM} and elastic deformation decrease. Due to the nature of the experiments, all μ_{TM} are higher than expected for a clean Si_3N_4 tip and a hydrocarboned surface. As the F_f vs. F_v curves remove the monolayer from the surface, we expect disordered AA molecules to be on the tip as the next F_f vs. F_v curve begins, fact that increases the interactions between the two surfaces. Nevertheless the μ_{TM} tendency to decrease is clear, as it also is the sensitivity of these measurements to the molecular packing density.

Dealing with the region c) in Fig. 5 inset, preliminary experiments performed on clean mica rendered friction coefficients of 0.17±0.03 in air, while μ_S ranges from 0.73 to 0.42. In this case, it is difficult to

precisely define the tip-sample interface, as the AA monolayer is ruptured and individual molecules are scattered on the surface sample, increasing the frictional interaction. Interestingly, μ_S strongly depends on the extraction pressure, reducing its value as the area per molecule and the tilting angle decreases. As the only difference between the samples is the quantity of disordered AA molecules that are still in the scanning area, the packing density plays an important role again; at low extraction pressures, the weak interaction between molecules let them scatter individually on the scanning area, increasing the number of interactions between the molecules stuck on the tip and the sample. Instead, as extraction pressure increases, it is more difficult to break the individual interactions between molecules and we propose that they are expulsed in clusters, leaving a cleaner substrate with frictional properties closer to those of bare mica. According to this, a previous work demonstrated the interplay between the packing density and the molecular expulsion mechanism, concluding that a tight structure leads to a brittle structural break, while a loose packing is more prone to deform plastically under the exertion of a $F_\downarrow$[13].

CONCLUSIONS

The analysis of AFM topographic images of AA monolayers extracted at different pressures reveals that the tilting angle of the molecules decreases as their pressure increases. Moreover, the tilting is not continuous but discrete and equals 50°, 50°/34° and 34°/22° for samples extracted at 1, 15 and 35 mN/m respectively, being in excellent accordance with the 2D chain interlocking model.

Force Spectroscopy measurements show that $F_\downarrow$ strongly depends on the monolayer phase detected in the surface pressure vs. area per molecule isotherm (solid phase at 35 mN/m breaks at 22.94±5.49 nN while liquid condensed phase at 15 mN/m breaks at 15.34±4.94 nN) but also on the tilting angle differences observed in a same phase. Consequently, $F_\downarrow$ can be considered as a fingerprint for the structural conformation of monolayers due to its sensitivity to different molecular orientations. Moreover, as the obtained $F_\downarrow$ values are fully quantitative, they can be used to assess the different forces involved in the monolayer cohesion. In this particular case, the $F_\downarrow$ increment with extraction pressure can not be explained only as a function of the increasing van der Waals interaction between chains due to the tilting angle reduction. Then, the electrostatic and H-bond interactions between the carboxylic acid headgroups play an important role in the monolayer mechanical resistance. Further works should be devoted to study the dependence of $F_\downarrow$ with different headgroups, pH conditions and subphase ions so as to probe the contribution of these factors to the nanomechanical properties of fatty acid monolayers.

Friction experiments show that the tribological properties of these monolayers highly depend on the applied $F_\downarrow$ and 3 regimes are observed. These regimes correspond with the tip sliding on top of the alkyl chains, the tip plastically deforming the monolayer and inducing a molecular tilting and finally rupturing the monolayer and contacting the substrate. Interestingly, the $F_\downarrow$ that the monolayer can

withstand before deforming plastically increases with extraction pressure, fact that highlights the sensitivity of Lateral Force Microscopy to the sample molecular ordering.

ACKNOWLEDGEMENT

G.O. thanks Matt Brukman and Robert Carpick (University of Wisconsin, WI) for providing the Matlab scripts to analyze friction data and Mickey Huson (CSIRO) for the AFM Force Volume Data Analysis Software. This work has been supported by Generalitat de Catalunya trough project 2002PIRA 00167, and by MCYT through projects CTQ2004-08046-C02-01 and CTQ2004-08046-C02-02.

REFERENCES

1. Blodgett, K. B. *J. Am. Chem. Soc.* **1935**, *57*, 1007.
2. Kiessling, V.; Crane, J. M.; Tamm, L. K. *Biophys. J.* **2006**, *91*, 3313.
3. Tao, A.; Kim, F.; Hess, C.; Goldberger, J.; He, R. R.; Sun, Y. G.; Xia, Y. N.; Yang, P. D. *Nano Lett.* **2003**, *3*, 1229.
4. Cong, P.; Nanao, H.; Igari, T.; Mori, S. *Appl. Surf. Sci.* **2000**, *167*, 152.
5. Ren, S. L.; Yang, S. R.; Wang, J. Q.; Liu, W. M.; Zhao, Y. P. *Chem. Mat.* **2004**, *16*, 428.
6. Leggett, G. J. *Anal. Chim. Acta* **2003**, *479*, 17.
7. Carpick, R. W.; Salmeron, M. *Chem. Rev.* **1997**, *97*, 1163.
8. Bhushan, B.; Israelachvili, J. N.; Landman, U. *Nature* **1995**, *374*, 607.
9. Krim, J. *Surf. Sci.* **2002**, *500*, 741.
10. Gnecco, E.; Bennewitz, R.; Gyalog, T.; Meyer, E. *Journal of Physics-Condensed Matter* **2001**, *13*, R619.
11. Takano, H.; Kenseth, J. R.; Wong, S. S.; O'Brien, J. C.; Porter, M. D. *Chem. Rev.* **1999**, *99*, 2845.
12. Grant, L. M.; Tiberg, F. *Biophys. J.* **2002**, *82*, 1373.
13. Oncins, G.; Garcia-Manyes, S.; Sanz, F. *Langmuir* **2005**, *21*, 7373.
14. Garoff, S.; Deckman, H. W.; Dunsmuir, J. H.; Alvarez, M. S.; Bloch, J. M. *Journal de Physique* **1986**, *47*, 701.
15. Matsumoto, M.; Tanaka, K.; Azumi, R.; Kondo, Y.; Yoshino, N. *Langmuir* **2003**, *19*, 2802.
16. Mori, O.; Imae, T. *Langmuir* **1995**, *11*, 4779.
17. Evenson, S. A.; Badyal, J. P. S.; Pearson, C.; Petty, M. C. *J. Phys. Chem.* **1996**, *100*, 11672.
18. Kajiyama, T.; Oishi, Y.; Hirose, F.; Shuto, K.; Kuri, T. *Langmuir* **1994**, *10*, 1297.
19. Leuthe, A.; Chi, L. F.; Riegler, H. *Thin Solid Films* **1994**, *243*, 351.
20. Chunbo, Y.; Desheng, D.; Zuhong, L.; Juzheng, L. *Coll. Surf. A* **1999**, *150*, 1.
21. Hartig, M.; Chi, L. F.; Liu, X. D.; Fuchs, H. *Thin Solid Films* **1998**, *329*, 262.
22. Oishi, Y.; Umeda, T.; Kuramori, M.; Suehiro, K. *Langmuir* **2002**, *18*, 945.
23. Oishi, Y.; Kasagi, T.; Kuramori, M.; Suehiro, K. *Coll. Surf. A* **2000**, *169*, 171.
24. Meyer, E.; Overney, R.; Brodbeck, D.; Howald, L.; Luthi, R.; Frommer, J.; Guntherodt, H. J. *Phys. Rev. Lett.* **1992**, *69*, 1777.
25. Kondrashkina, E. A.; Hagedorn, K.; Vollhardt, D.; Schmidbauer, M.; Kohler, R. *Langmuir* **1996**, *12*, 5148.
26. Oncins, G.; Torrent-Burgues, J.; Sanz, F. *Tribol. Lett.* **2006**, *21*, 175.
27. Tsukruk, V. V.; Bliznyuk, V. N.; Hazel, J.; Visser, D.; Everson, M. P. *Langmuir* **1996**, *12*, 4840.
28. Florin, E. L.; Rief, M.; Lehmann, H.; Ludwig, M.; Dornmair, C.; Moy, V. T.; Gaub, H. E. *Biosensors & Bioelectronics* **1995**, *10*, 895.

29 Developed in CSIRO (Australia's Commonwealth Scientific and Industrial Research Organisation) by Dr Mickey Huson Contact mickey huson@csiro au

30 Ogletree, D F , Carpick, R W , Salmeron, M *Rev Sci Instrum* **1996**, *67*, 3298

31 Brukman, M J , Marco, G O Dunbar, T D , Boardman, L D , Carpick, R W *Langmuir* **2006**, *22*, 3988

32 The scripts are available for non-commercial use at http //mandm engr wisc edu/faculty_pages_carpick/toolbox htm

33 This value is measured perpendicular to the alkyl chains, while the distance measurements extracted from the average area per molecule are measured parallel to the surface

34 Israelachvili, J N *Intermolecular Surface Forces*, 1 ed , Academic Press London, 1985, 88-89
35 Rabe, J P , Swalen, J D , Outka, D A , Stohr, J *Thin Solid Films* **1988**, *159*, 275

36 Outka, D A , Stohr, J , Rabe, J P , Swalen, J D *J Chem Phys* **1988**, *88*, 4076

37 Rabe, J P , Novotny, V , Swalen, J D Rabolt, J F *Thin Solid Films* **1988**, *159*, 359

38 Rabe, J P Swalen, J D , Rabolt J F *J Chem Phys* **1987**, *86* 1601

39 Ahn D J , Franses, E I *J Phys Chem* **1992**, *96*, 9952

40 Robinson, I Jarvis, D J , Sambles, J R *Journal of Physics D-Applied Physics* **1991** *24*, 347

41 Outka D A , Stohr, J , Rabe, J P , Swalen, J D Rotermund, H H *Phys Rev Lett* **1987**, *59*, 1321

42 Ulman, A , Eilers, J E , Tillman, N *Langmuir* **1989**, *5* 1147

43 Wurger, A *Phys Rev Lett* **1999**, *83*, 1696

44 Barrena, E , Ocal, C , Salmeron, M *J Chem Phys* **2000**, *113*, 2413

45 The depicted tilting angles correspond to m=1 and n=0 (18°), n=1/2 (22°) n=1 (32°), n=3/2 (41°) and n=2 (48°) For a further description of the method see ref 44

46 Pignataro, B , Panebianco, S , Consalvo, C , Licciardello, A *Surface and Interface Analysis* **1999**, *27*, 396

47 Domke, J , Radmacher, M *Langmuir* **1998**, *14*, 3320

48 Schneider, J , Barger, W , Lee, G U *Langmuir* **2003**, *19*, 1899

49 Kunneke, S , Kruger D , Janshoff, A *Biophys J* **2004**, *86*, 1545

50 Loi, S , Sun, G , Franz, V , Butt, H J *Phys Rev E* **2002**, *66*

51 Franz, V , Loi S , Muller, H , Bamberg, E , Butt, H H *Coll Surf B* **2002**, *23*, 191

52 Garcia-Manyes, S , Oncins, G , Sanz, F *Biophys J* **2005**, *89* 4261

53 Garcia-Manyes, S , Oncins, G , Sanz, F *Biophys J* **2005**, *89*, 1812

54 32° and 48° correspond to the slip of 1 and 2 notches respectively For 22°, it was considered a ½ notch slippage, possibility experimentally confirmed in ref 43, resulting in a van der Waals interaction loss of 3 45 kJ/mol

55 The molecular area obtained during the Langmuir Blodgett transfer (27, 22 and 19 $Å^2$ for 1, 15 and 35 mN/m samples) was included in the calculation so as to normalize F_t and E_t to the same number of affected AA molecules

56 Du, X Z , Shi, B , Liang, Y Q *Langmuir* **1998**, *14*, 3631

57 Du, X Z , Liang, Y Q *J Chem Phys* **2004**, *120*, 379

58 Umemura, J , Takeda, S , Hasegawa, T , Takenaka, T *Journal of Molecular Structure* **1993**, *297*, 57

59 Ren, Y Z , Asanuma, M , Iimura, K , Kato, T *J Chem Phys* **2001**, *114*, 923

60 Butt, H J *Biophys J* **1991**, *60*, 777

61 Tippmann-krayer, P , Mohwald, H *J Phys Chem* **1992**, *96*, 5220

62 Wang, Y C , Du, X Z , Guo, L , Liu, H J *J Chem Phys* **2006**, *124*

63 Gloslı, J N , Mcclelland, G M *Phys Rev Lett* **1993**, *70*, 1960

64 Barrena, E , Ocal, C . Salmeron, M *J Chem Phys* **1999**, *111*, 9797

65 Kim, H I , Graupe, M , Oloba, O , Koini, T , Imaduddin, S , Lee, T R , Perry, S S *Langmuir* **1999**, *15*, 3179

LIST OF FIGURES

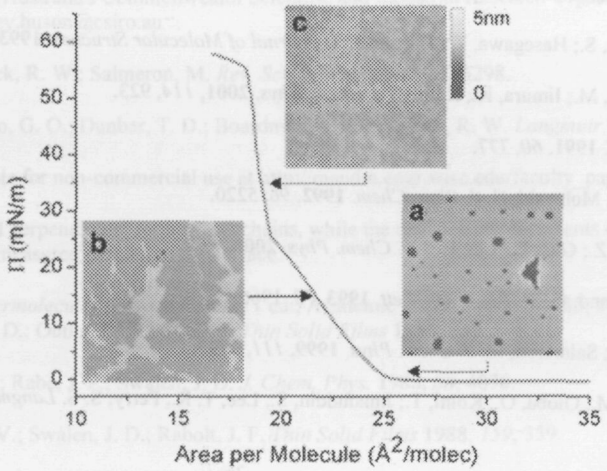

Figure 1. AA surface pressure vs. area per molecule isotherm (24°C). 5 x 5 μm² AFM contact mode images of AA monolayers extracted at a) 1 mN/m, b) 15 mN/m and c) 35 mN/m. The voids observed in image a) correspond to the mica surface.

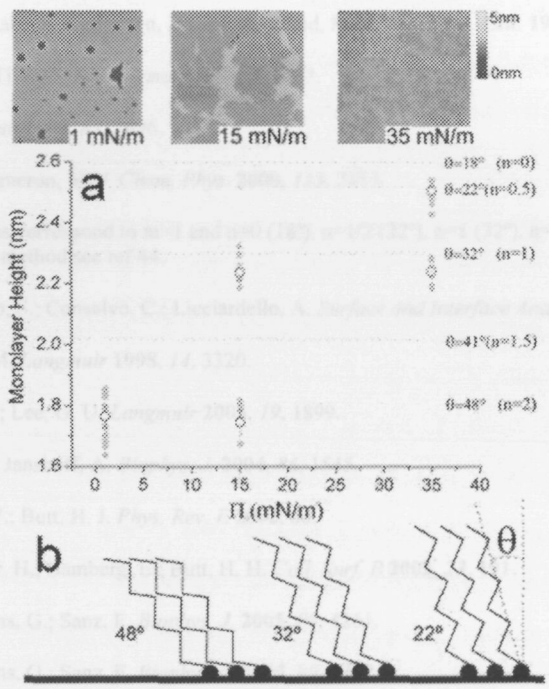

Figure 2. a) AA monolayer height measurements vs. extraction pressure. Grey dots correspond to individual measurements and white dots are mean values. Error bars are calculated as $2s/\sqrt{N}$, being s the standard deviation and N the number of individual measurements for each phase in each extraction pressure ($15<N<20$). Dotted lines mark the monolayer height and tilting angles (θ) predicted by Barrena et al.[44], where n is the tilting step in the next-neighbor AA molecule direction. b) Schematics of the three phases detected in the studied samples.

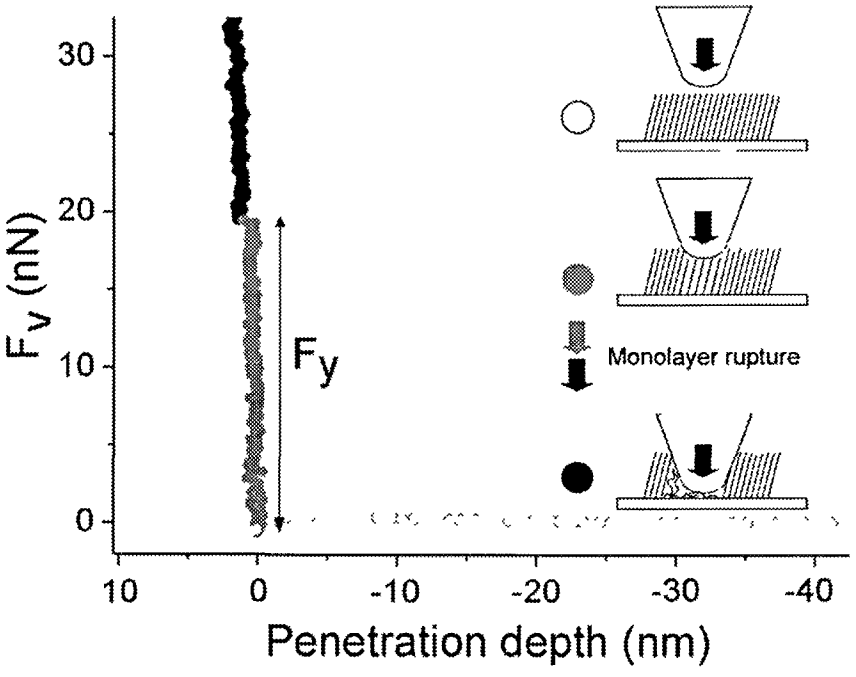

Figure 3. F_v **vs. penetration depth curve on an AA monolayer extracted at 35 mN/m. White dots: non-contact. Grey dots: sample compression and monolayer rupture (F_y). Black dots: hard contact between tip and mica surface.**

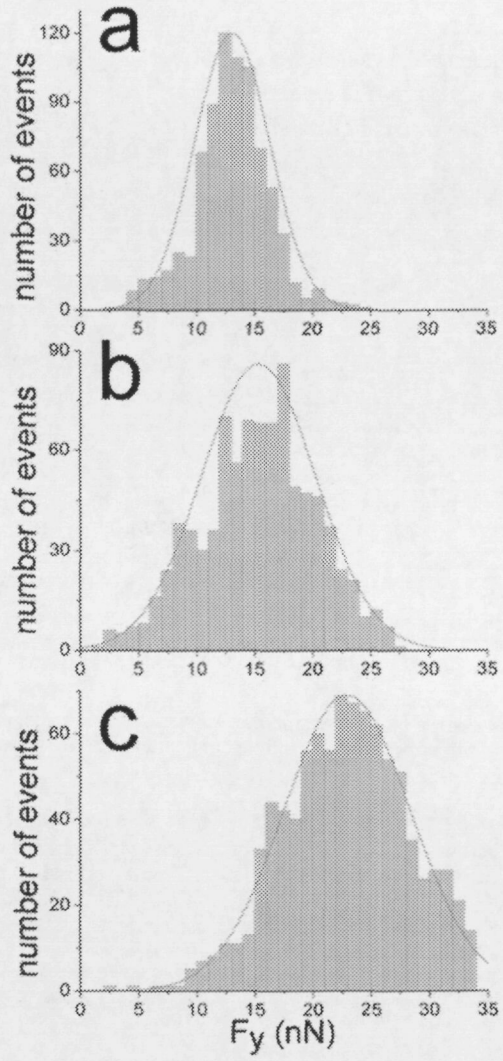

Figure 4. Histograms of AA monolayer breakthrough force (F_y) for samples extracted at a) 1 mN/m, b) 15 mN/m and c) 35 mN/m where 400<N<600, being N the number of individual F_y measurements at every extraction pressure. Gaussian fitting values: a) 13.07±3.24 nN, b) 15.34±4.94 nN and c) 22.94±5.49 nN where the error is the standard deviation.

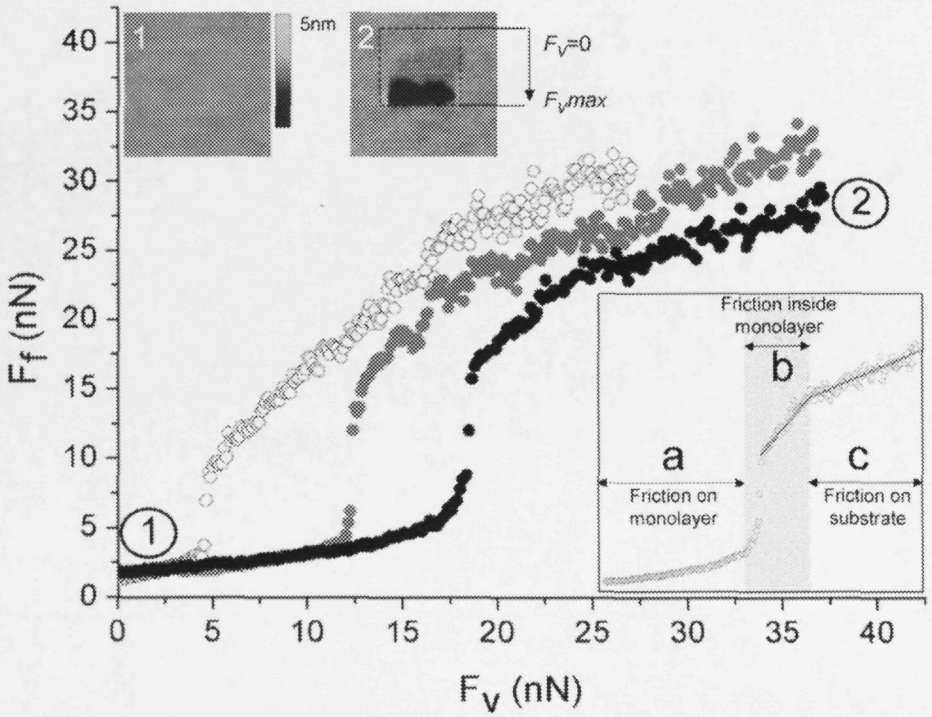

Figure 5. F_f vs. F_v curves obtained on AA monolayers extracted at 1 mN/m (white dots), 15 mN/m (grey dots) and 35 mN/m (black dots). Inset: F_f vs. F_v curve scheme with the three friction regimes that goes from soft contact with the monolayer (a) to sample rupture (c). Image 1 (top left): topographic image of the sample before performing the F_f vs. F_v curve. Image 2: after performing the F_f vs. F_v curve.

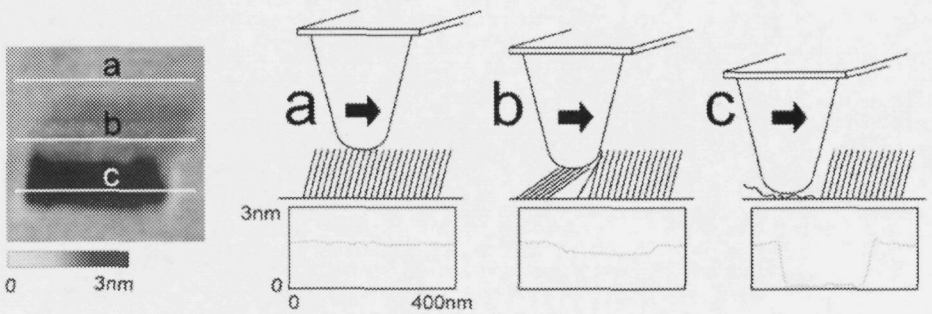

Figure 6. Proposed model for the tip-sample interaction as F_v increases. a) elastic sample deformation, no structural changes (low friction). b) molecular tilting (plastic deformation) induced by the pressure exerted by the tip, resulting in a friction increment. c) monolayer rupture and contact with the substrate. These regimes correspond with the a), b) and c) regions of the Fig. 5 inset. The topographic image was captured after performing a F_f vs. F_v curve on a AA monolayer extracted at 1mN/m (scanning direction: up-down). The topographic sections under each cartoon are marked as white lines in the image.

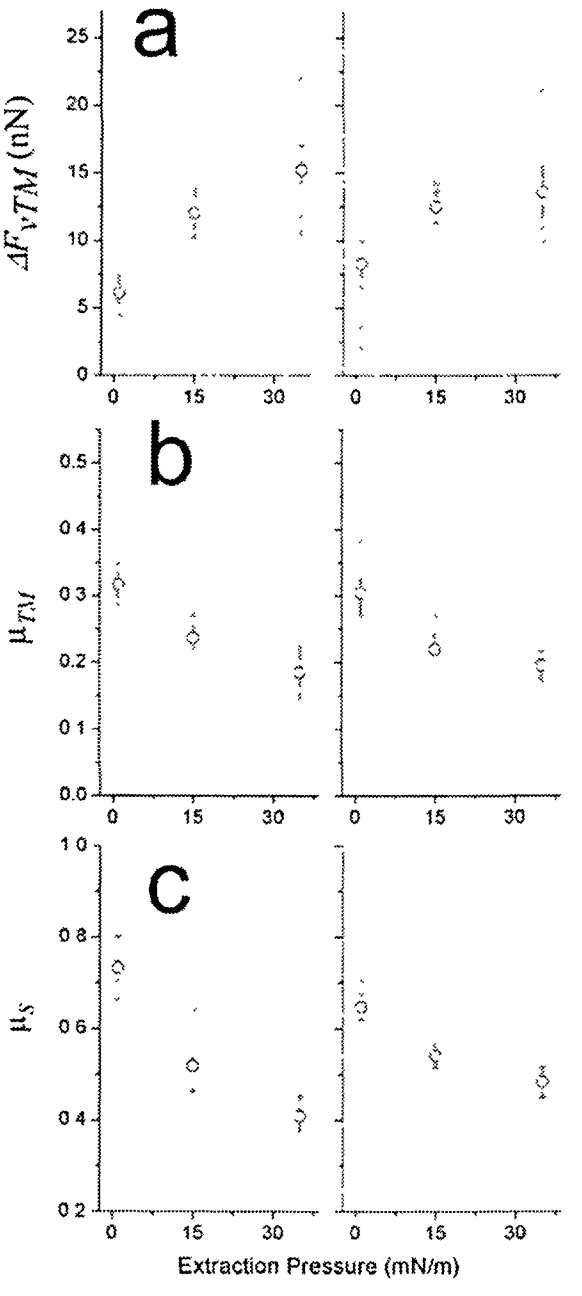

Figure 7. F_j **vs.** F_v **curve analysis, where a)** ΔF_{vTM} **vs. extraction pressure. b)** μ_{TM} **vs. extraction pressure and c)** μ_S **vs. extraction pressure. The measurements were performed on two different samples with two different tips. Grey dots stand for individual measurements and white dots are the mean values. The error bars stand for** $2s/\sqrt{N}$**., being** N **the number of individual measurements.**

4.6.5 Nanotribological Properties of Alkanephosphonic Acid Self-Assembled Monolayers on Aluminum Oxide: Effects of Fluorination and Substrate Crystallinity

M.J. Brukman[a], G. Oncins[b], T.D. Dunbar[c], L.D. Boardman[c], R.W. Carpick[a]

[a]Department of Engineering Physics, University of Wisconsin, Madison, Wisconsin 53706

[b]Department of Physical Chemistry, Universitat de Barcelona and Center of Nanobioengineering of Catalonia (CREBEC), Martí i Franquès 1, 08028 Barcelona, Spain

[c]3M Corporate Research Materials Laboratory, St. Paul, Minnesota 55144

Langmuir 22(9), (2006), 3988-3998.

4.6.5.1 Summary

Alkanephosphonic acid monolayers, despite not being so widely used as alkanethiols and alkanesilanes in friction-related applications, present very interesting properties. Their main advantage is that they strongly bind to several metal oxides and metallic surfaces, providing durable monolayers, for example, on aluminum and aluminum oxide, which are important structural materials in the development of MEMS and NEMS.

This work was really challenging from the beginning, as our goals were focused on two different directions; first of all, it was necessary to develop an experimental protocol to obtain reproducible and meaningful quantitative LFM measurements with different AFM tips which, I must confess, is the darkest art of the AFM nanotribologist. Secondly, we wanted to detect if the monolayer substrate

crystallographic plane modifies the friction response of the layer. To do that, we prepared samples on amorphous alumina and on the C and R crystallographic planes of single crystal α-alumina.

The results can be summarized as follows:

- *An experimental method to obtain reproducible LFM measurements was developed, consisting on the chemical equilibration of the tip and the sample prior to acquiring friction data.*

- *Monolayers deposited on amorphous alumina present a μ value lower than that of the monolayers deposited on C and R alumina. We proposed that the crystallographic planes force the phosphonic acid groups to bind in specific surface sites, which alters the free packing of the monolayer, while the amorphous alumina surface does not constrain the molecular binding to the substrate and the resulting monolayer is more compact and, consequently, presents lower μ values.*

- *Two different sets of alkanephosphonic acid molecules were tested: with fully hydrogenated and partially fluorinated chains. Although all these coatings present a lower μ value than the bare alumina surface, the fluorinated monolayers have a higher μ value than the hydrogenated ones. It was proposed that the bulky F- groups are responsible for the lack of compactness of the fluorinated layers, fact that promotes pathways to dissipate energy during sliding and reduces the lubricant nature of the coating.*